Article

Bimetallic Effects in Homopolymerization of Styrene and Copolymerization of Ethylene and Styrenic Comonomers: Scope, Kinetics, and Mechanism

Neng Guo, Charlotte L. Stern, and Tobin J. Marks

J. Am. Chem. Soc., **2008**, 130 (7), 2246-2261 • DOI: 10.1021/ja076407m

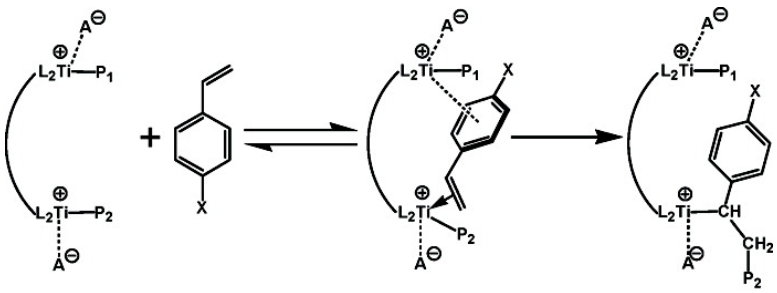

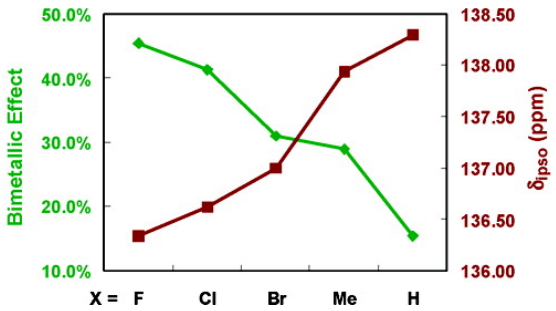

More About This Article

Additional resources and features associated with this article are available within the HTML version:

- Supporting Information
- Links to the 5 articles that cite this article, as of the time of this article download
- Access to high resolution figures
- Links to articles and content related to this article
- Copyright permission to reproduce figures and/or text from this article

View the Full Text HTML

J|A|C|S
ARTICLES
Published on Web 01/26/2008

Bimetallic Effects in Homopolymerization of Styrene and Copolymerization of Ethylene and Styrenic Comonomers: Scope, Kinetics, and Mechanism

Neng Guo, Charlotte L. Stern, and Tobin J. Marks*

Department of Chemistry, Northwestern University, Evanston, Illinois 60208-3113

Received August 25, 2007; E-mail: t-marks@northwestern.edu

Abstract: This contribution describes the homopolymerization of styrene and the copolymerization of ethylene and styrenic comonomers mediated by the single-site bimetallic "constrained geometry catalysts" (CGCs), (μ-CH_2CH_2-3,3′){(η^5-indenyl)[1-Me_2Si(^{t}BuN)]($TiMe_2$)}$_2$ [EBICGC($TiMe_2$)$_2$; **Ti$_2$**], (μ-CH_2CH_2-3,3′){(η^5-indenyl)[1-Me_2Si(^{t}BuN)]($ZrMe_2$)}$_2$ [EBICGC($ZrMe_2$)$_2$; **Zr$_2$**], (μ-CH_2-3,3′){(η^5-indenyl)[1-Me_2Si(^{t}BuN)]($TiMe_2$)}$_2$ [MBICGC($TiMe_2$)$_2$; **C1-Ti$_2$**], and (μ-CH_2-3,3′){(η^5-indenyl)[1-Me_2Si(^{t}BuN)]($ZrMe_2$)}$_2$ [MBICGC($ZrMe_2$)$_2$; **C1-Zr$_2$**], in combination with the borate activator/cocatalyst $Ph_3C^+B(C_6F_5)_4^-$ (**B$_1$**). Under identical styrene homopolymerization conditions, **C1-Ti$_2$** + **B$_1$** and **Ti$_2$** + **B$_1$** exhibit ~65 and ~35 times greater polymerization activities, respectively, than does monometallic [1-Me_2Si(3-ethylindenyl)(^{t}BuN)]$TiMe_2$ (**Ti$_1$**) + **B$_1$**. **C1-Zr$_2$** + **B$_1$** and **Zr$_2$** + **B$_1$** exhibit ~8 and ~4 times greater polymerization activities, respectively, than does the monometallic control [1-Me_2Si(3-ethylindenyl)(^{t}BuN)]$ZrMe_2$ (**Zr$_1$**) + **B$_1$**. NMR analyses show that the bimetallic catalysts suppress the regiochemical insertion selectivity exhibited by the monometallic analogues. In ethylene copolymerization, **Ti$_2$** + **B$_1$** enchains 15.4% more styrene (**B**), 28.9% more 4-methylstyrene (**C**), 45.4% more 4-fluorostyrene (**D**), 41.2% more 4-chlorostyrene (**E**), and 31.0% more 4-bromostyrene (**F**) than does **Ti$_1$** + **B$_1$**. This observed bimetallic chemoselectivity effect follows the same general trend as the π-electron density on the styrenic *ipso* carbon (**D** > **E** > **F** > **C** > **B**). Kinetic studies reveal that both **Ti$_2$** + **B$_1$** and **Ti$_1$** + **B$_1$**-mediated ethylene−styrene copolymerizations follow second-order Markovian statistics and tend to be alternating. Moreover, calculated reactivity ratios indicate that **Ti$_2$** + **B$_1$** favors styrene insertion more than does **Ti$_1$** + **B$_1$**. All the organozirconium complexes (**C1-Zr$_2$**, **Zr$_2$**, and **Zr$_1$**) are found to be incompetent for ethylene−styrene copolymerization, yielding only mixtures of polyethylene and polystyrene. Model compound (μ-CH_2CH_2-3,3′){(η^5-indenyl)[1-Me_2Si(^{t}BuN)][Ti(CH_2Ph)$_2$]}$_2$ {EBICGC[Ti(CH_2Ph)$_2$]$_2$; **Ti$_2$-(CH$_2$Ph)$_4$**} was designed, synthesized, and structurally characterized. In situ activation studies with cocatalyst $B(C_6F_5)_3$ suggest an η^1-coordination mode for the benzyl groups, thus supporting the proposed polymerization mechanism. For ethylene−styrene copolymerization, polar solvents are found to increase copolymerization activities and coproduce atactic polystyrene impurities in addition to ethylene-co-styrene, without diminishing the comonomer incorporation selectivity. Both homopolymerization and copolymerization results argue that substantial cooperative effects between catalytic sites are operative.

Introduction

Intensive recent research efforts have focused on discovering unique or more efficient homogeneous catalytic processes which benefit from cooperative effects between adjacent active centers in multinuclear metal complexes.[1] In ideal cases, these mimic enzymatic capabilities in creating high local reagent concentrations and special, conformationally advantaged active site−substrate interactions.[2] For single-site olefin polymerization catalysts,[3] we recently reported that $-CH_2CH_2-$ (**Ti$_2$**, **Zr$_2$**) and $-CH_2-$ (**C1-Ti$_2$**, **C1-Zr$_2$**) linked bimetallic "constrained geometry catalysts" (CGCs)[4] exhibit remarkable nuclearity effects in terms of chain branch formation, α-olefin comonomer enchainment selectivity, and molecular weight enhancement compared to their mononuclear counterparts (**Ti$_1$**, **Zr$_1$**) (Chart 1).[5] For ethylene copolymerizations, we speculated that when

(1) (a) Li, C.; Chen, L.; Garland, M. *J. Am. Chem. Soc.* **2007**, *129*, 13327−13334. (b) Weng, Z.; Teo, S.; Liu, Z.; Hor, T. S. A. *Organometallics* **2007**, *26*, 2950−2952. (c) Sammis, G. M.; Danjo, H.; Jacobsen, E. N. *J. Am. Chem. Soc.* **2004**, *126*, 9928−9929. (d) Moore, D. R.; Cheng, M.; Lobkovsky, E. B.; Coates, G. W. *J. Am. Chem. Soc.* **2003**, *125*, 11911−11924. (e) Trost, B. M.; Mino, T. *J. Am. Chem. Soc.* **2003**, *125*, 2410−2411. (f) Jacobsen, E. N. *Acc. Chem. Res.* **2000**, *33*, 421−431. (g) Molenveld, P.; Engbersen, J. F. J.; Reinhoudt, D. N. *Chem. Soc. Rev.* **2000**, *29*, 75−86. (h) Konsler, R. G.; Karl, J.; Jacobsen, E. N. *J. Am. Chem. Soc.* **1998**, *120*, 10780−10781. (i) Molenveld, P.; Kapsabelis, S.; Engbersen, J. F. J.; Reinhoudt, D. N. *J. Am. Chem. Soc.* **1997**, *119*, 2948−2949. (j) Mathews, R. C.; Howell, D. H.; Peng, W.-J.; Train, S. G.; Treleaven, W. D.; Stanley, G. G. *Angew. Chem., Int. Ed. Engl.* **1996**, *35*, 2253−2256. (k) Sawamura, M.; Sudoh, M.; Ito, Y. *J. Am. Chem. Soc.* **1996**, *118*, 3309−3310.

(2) (a) Collman, J. P.; Boulatov, R.; Sunderland, C. J.; Fu, L. *Chem. Rev.* **2004**, *104*, 561−588. (b) Krishnan, R.; Voo, J. K.; Riordan, C. G.; Zahkarov, L.; Rheingold, A. L. *J. Am. Chem. Soc.* **2003**, *125*, 4422−4423. (c) Bruice, T. C. *Acc. Chem. Res.* **2002**, *35*, 139−148. (d) Bruice, T. C.; Benkovic, S. J. *Biochemistry* **2000**, *39*, 6267−6274 and references therein. (e) O'Brien, D. P.; Entress, R. M. N.; Matthew, A. C.; O'Brien, S. W.; Hopkinson, A.; Williams, D. H. *J. Am. Chem. Soc.* **1999**, *121*, 5259−5265. (f) Carazo-Salas, R. E.; Guarguaglini, G.; Gruss, O. J.; Segref, A.; Karsenti, E.; Mattaj, L. W. *Nature* **1999**, *400*, 178−181. (g) Menger, F. M. *Acc. Chem. Res.* **1993**, *26*, 206−212 and references therein. (h) Page, M. I. In *The Chemistry of Enzyme Action*; Page, M. I., Ed.; Elsevier: New York, 1984; pp 1−54.

10.1021/ja076407m CCC: $40.75

Chart 1

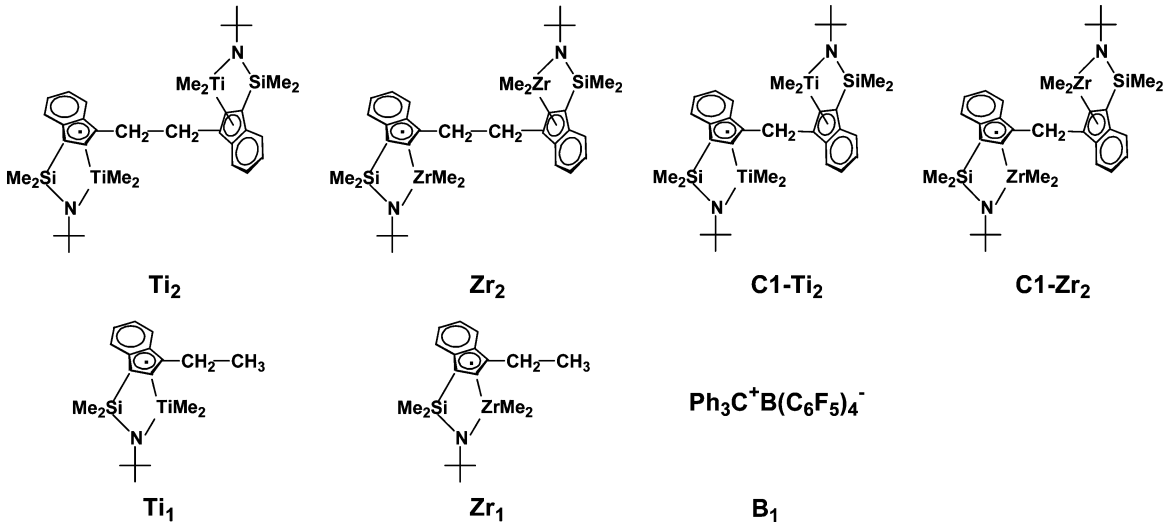

Scheme 1. Proposed Mechanistic Scenario for Enhanced Comonomer Enchainment by Bimetallic Catalysts

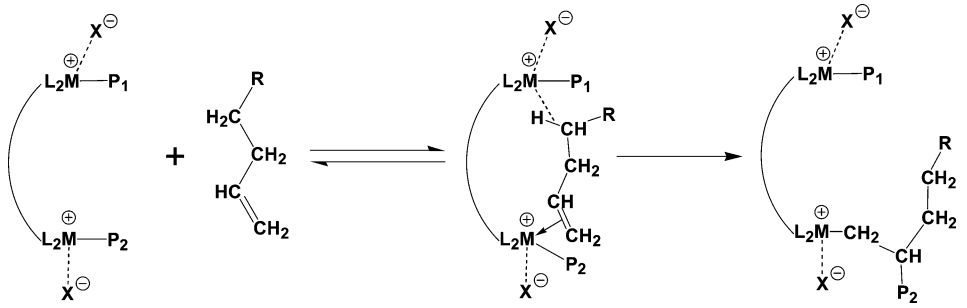

the double bond of the alkene comonomer binds to the first metal center, the second d^0, highly electrophilic metal center can engage in secondary, possibly agostic interactions[6] with sp^3 sites, leading to enhanced comonomer binding affinity and activating capacity (Scheme 1). Density functional theory (DFT/B3LYP) calculations reveal that this agostic interaction contributes ~2 kcal/mol stabilization to the coordinated bimetallic α-olefin complex.[7] The next intriguing question is whether these binuclear cooperative enchainment effects are more likely to mediate unusual polymerization patterns involving monomers, such as styrenes and dienes, with more basic secondary coordinating moieties.

Over the past several decades, ethylene−styrene copolymers have received great attention due to their impressive viscoelastic behavior, mechanical properties, and compatibilities with a wide range of other polymeric materials, arising from the introduction of aromatic functional groups into the polyethylene backbone.[8] Initial attempts to copolymerize ethylene and styrene via heterogeneous Ziegler−Natta processes proved largely unsuc-

(3) For recent reviews of single-site olefin polymerization, see: (a) Marks, T. J. *Proc. Natl. Acad. Sci. U.S.A* **2006**, *103* (Special Feature on Polymerization). (b) Li, H.; Marks, T. J. *Proc. Natl. Acad. Sci. U.S.A* **2006**, *103*, 15295−15302. (c) Severn, J. R.; Chadwick, J. C.; Duchateau, R.; Friederichs, N. *Chem. Rev.* **2005**, *105*, 4073−4147. (d) Kaminsky, W. *J. Polym. Sci., Part A: Polym. Chem.* **2004**, *42*, 3911−3921. (e) Gibson, V. C.; Spitzmesser, S. K. *Chem. Rev.* **2003**, *103*, 283−316. (f) Pédeutour, J.-N.; Radhakrishnan, K.; Cramail, H.; Deffieux, A. *Macromol. Rapid Commun.* **2001**, *22*, 1095−1123. (g) Gladysz, J. A. *Chem. Rev.* **2000**, *100*, (special issue on Frontiers in Metal-Catalyzed Polymerization). (h) Marks, T. J.; Stevens, J. C. *Top. Catal.* **1999**, *15*, and references therein. (i) Britovsek, G. J. P.; Gibson, V. C.; Wass, D. F. *Angew. Chem. Int. Ed.* **1999**, *38*, 428−447. (j) Kaminsky, W.; Arndt, M. *Adv. Polym. Sci.* **1997**, *127*, 144−187. (k) Bochmann, M. *J. Chem. Soc., Dalton Trans.* **1996**, 255−270. (l) Brintzinger, H.-H.; Fischer, D.; Mülhaupt, R.; Rieger, B.; Waymouth, R. M. *Angew. Chem., Int. Ed.* **1995**, *34*, 1143−1170. (m) *Catalyst Design for Tailor-Made Polyolefins*; Soga, K., Terano, M., Eds.; Elsevier: Tokyo, 1994. (n) Marks, T. J. *Acc. Chem. Res.* **1992**, *25*, 57−65.

(4) For constrained-geometry catalysts, see: (a) Iedema, P. D.; Hoefsloot, H. C. J. *Macromolecules* **2003**, *36*, 6632−6644. (b) Klosin, J.; Kruper, W. J., Jr.; Nickias, P. N.; Roof, G. R.; De Waele, P.; Abboud, K. A. *Organometallics* **2001**, *20*, 2663−2665. (c) McKnight, A. L.; Waymouth, R. M. *Chem. Rev.* **1998**, *98*, 2587−2598. (d) Lai, S. Y.; Wilson, J. R.; Knight, G. W.; Stevens, J. C. *WO-93/08221*, **1993**.

(5) (a) Li, H.; Li, L.; Schwartz, D. J.; Metz, M. V.; Marks, T. J.; Liable-Sands, L.; Rheingold, A. L. *J. Am. Chem. Soc.* **2005**, *127*, 14756−14768. (b) Li, H.; Stern, C. L.; Marks, T. J. *Macromolecules* **2005**, *38*, 9015−9027. (c) Li, H.; Li, L.; Marks, T. J. *Angew. Chem., Int. Ed.* **2004**, *37*, 4937−4940. (d) Wang, J.; Li, H.; Guo, N.; Li, L.; Stern, C. L.; Marks, T. J. *Organometallics* **2004**, *23*, 5112−5114. (e) Guo, N.; Li, L.; Marks, T. J. *J. Am. Chem. Soc.* **2004**, *126*, 6542−6543. (f) Li, H.; Li, L.; Marks, T. J.; Liable-Sands, L.; Rheingold, A. L. *J. Am. Chem. Soc.* **2003**, *125*, 10788−10789. (g) Abramo, G. P.; Li, L.; Marks, T. J. *J Am. Chem. Soc.* **2002**, *124*, 13966−13967. (h) Li, L.; Metz, M. V.; Li, H.; Chen, M.-C.; Marks, T. J.; Liable-Sands, L.; Rheingold, A. L. *J. Am. Chem. Soc.* **2002**, *124*, 12725−12741.

(6) (a) Scherer, W.; McGrady, G. S. *Angew. Chem., Int. Ed.* **2004**, *43*, 1782−1806. (b) Prosenc, M. H.; Brintzinger, H. H. *Organometallics* **1997**, *16*, 3889−3894. (c) Grubbs, R. H.; Coates, G. W. *Acc. Chem. Res.* **1996**, *29*, 85−93. (d) Prosenc, M. H.; Janiak, C.; Brintzinger, H. H. *Organometallics* **1992**, *11*, 4036−4041. (e) Cotter, W. D.; Bercaw, J. E. *J. Organomet. Chem.* **1991**, *417*, C1−C6. (f) Krauledat, H.; Brintzinger, H. H. *Angew. Chem., Int. Ed. Engl.* **1990**, *29*, 1412−1413. (g) Piers, W. E.; Bercaw, J. E. *J. Am. Chem. Soc.* **1990**, *112*, 9406−9407. (h) Brookhart, M.; Green, M. L. H.; Wong, L. L. *Prog. Inorg. Chem.* **1988**, *36*, 1−124. (i) Clawson, L.; Soto, J.; Buchwald, S. L.; Steigerwald, M. L.; Grubbs, R. H. *J. Am. Chem. Soc.* **1985**, *107*, 3377−3378.

(7) Motta, A.; Fragala, I. L.; Marks, T. J. "Theoretical Investigation of Proximity Effects in Binuclear Catalysts for Olefin Polymerization" Poster Presentation at *the International Symposium on Relationships between Heterogeneous and Homogeneous Catalysis XIII*, Berkeley, CA July 16−20, 2007 and manuscript in preparation.

(8) (a) Chum, P. S.; Kruper, W. J.; Guest, M. J. *Adv. Mater.* **2000**, *12*, 1759−1767. (b) Cheung, Y. W.; Guest, M. J. *J. Polym. Sci.: Part B: Polym. Phys.* **2000**, *38*, 2976−2987. (c) Chen, H.; Guest, M. J.; Chum, S.; Hiltner, A.; Baer, E. *J. Appl. Polym. Sci.* **1998**, *70*, 109−119.

cessful, typically yielding homopolymer mixtures or copolymers with styrene incorporation <1 mol %.[9] The development of homogeneous single-site polymerization catalysts has led to a resurgence of interest in this field; however, challenges remain.[10−12] For Cp′TiXYZ-type catalysts[10] (Cp′ = substituted or unsubstituted η^5-cyclopentadienyl, indenyl, fluorenyl; X, Y, Z = halogen, alkyl, alkoxy, aryloxy, ketimide, etc. ligand), substantial quantities of homopolymer contaminants are coproduced in addition to ethylene−styrene copolymers, likely due to multiple active species, and in certain cases, the presence of excess cocatalyst. CGCTi catalysts represent another major advance in this field, producing ethylene−styrene copolymers exclusively; however styrene incorporation is invariably <50 mol %, regardless of the styrene:ethylene feed ratio. The copolymer obtained is described as "pseudo-random", because no head-to-tail styrene coupling is detected, even at relatively high levels of styrene incorporation.[12]

As a common, indispensable commodity plastic, polystyrene has also attracted extensive research efforts. Isotactic polystyrene was first synthesized by heterogeneous Ziegler−Natta catalysis[13] and was recently synthesized by homogeneous catalysis.[14,15] Cp′TiXYZ-type metallocene catalysts[16] and some other metallocene[11b,17] and nonmetallocene[18] catalysts are known to afford syndiotactic polystyrene; however, the nature of the catalytically active species and the mechanism of stereocontrol have not been unambiguously established. Mononuclear CGCTi catalysts exhibit marginal activity in styrene homopolymerization,[5e,12h] which is thought to be due to catalyst deactivation via arene "back-coordination"[19] in the 2,1-insertion product (**A**). It would

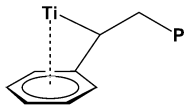

A

therefore be desirable to have a generalizable catalyst type, which, by tuning the symmetry of the ancillary ligand structure, could afford polystyrene products with efficient productivity and predetermined stereochemistry.

In a preliminary investigation,[5e] we briefly communicated that **Ti$_2$** not only exhibits far greater activity for styrene homopolymerizations than does **Ti$_1$**, and installs unusual 1,2-insertion regiochemistry[20] (up to ∼50%) in the initiation steps, but affords broad-range controllable styrene incorporation in ethylene−styrene copolymerizations, arguing that multinuclear cooperative catalysis indeed mediates unusual styrene polymerization patterns, although neither the scope, kinetics, nor mechanism were defined. In the present contribution, we investigate ethylene and styrene reactivity ratios for both **Ti$_2$**- and **Ti$_1$**-mediated copolymerizations, and extend comparative copolymerization studies to a selected variety of substituted styrenic comonomers (Chart 2) and to CGCZr catalysts (**C1-Zr$_2$**, **Zr$_2$**, and **Zr$_1$**) to fully characterize the scope and mechanism of this bimetallic effect. We also investigate the influence of metal−metal distance on these bimetallic cooperative effects in styrene homopolymerization and ethylene−styrene copolymerizations by comparing the properties of the methylene-bridged bimetallic catalysts **C1-Ti$_2$** and **C1-Zr$_2$** to the ethylene-bridged bimetallic variants **Ti$_2$** and **Zr$_2$**. In addition, model compound (μ-CH_2CH_2-3,3′){(η^5-

(9) (a) Aaltonen, P.; Seppälä, J.; Matilainen, L.; Leskelä, M. *Macromolecules* **1994**, *27*, 3136−3138. (b) Mani, P.; Burns, C. M. *Macromolecules* **1991**, *24*, 5475−5477. (c) Soga, K.; Lee, D. H.; Yanagihara, H. *Polym. Bull.* **1988**, *20*, 237−241.

(10) (a) Zhang, H.; Nomura, K. *Macromolecules* **2006**, *39*, 5266−5274. (b) Zhang, H.; Nomura, K. *J. Am. Chem. Soc.* **2005**, *127*, 9364−9365. (c) Nomura, K.; Okumura, H.; Komatsu, T.; Naga, N. *Macromolecules* **2002**, *35*, 5388−5395. (d) Nomura, K.; Komatsu, T.; Imanishi, Y. *Macromolecules* **2000**, *33*, 8122−8124. (e) Lee, D. H.; Yoon, K. B.; Kim, H. J.; Woo, S. S.; Noh, S. K. *J. Appl. Polym. Sci.* **1998**, *67*, 2187−2198. (f) Wu, Q.; Ye, Z.; Gao, Q.; Lin, S. *Macromol. Chem. Phys.* **1998**, *199*, 1715−1720. (g) Xu, G.; Lin, S. *Macromolecules* **1997**, *30*, 685−693. (h) Pellecchia, C.; Pappalardo, D.; D'Arco, M.; Zambelli, A. *Macromolecules* **1996**, *29*, 1158−1162. (i) Oliva, L.; Mazza, S.; Longo, P. *Macromol. Chem. Phys.* **1996**, *197*, 3115−3122. (j) Oliva, L.; Izzo, L.; Longo, P. *Macromol. Rapid Commun.* **1996**, *17*, 745−748. (k) Aaltonen, P.; Seppala, J. *Eur. Polym. J.* **1995**, *31*, 79−83. (l) Aaltonen, P.; Seppala, J. *Eur. Polym. J.* **1994**, *30*, 683−687. (m) Longo, P.; Grassi, A.; Oliva, L. *Macromol. Chem. Phys.* **1990**, *191*, 2387−2396.

(11) (a) Capacchione, C.; Proto, A.; Ebeling, H.; Mülhaupt, R.; Okuda, J. *J. Polym. Sci., Part A: Polym. Chem.* **2006**, *44*, 1908−1913. (b) Luo, Y.; Baldamus, J.; Hou, Z. *J. Am. Chem. Soc.* **2004**, *126*, 13910−13911. (c) Sernetz, F. G.; Mülhaupt, R.; Fokken, S.; Okuda, J. *Macromolecules* **1997**, *30*, 1562−1569.

(12) (a) Arriola, D. J.; Bokota, M.; Campbell, R. E., Jr.; Klosin, J.; LaPointe, R. E.; Redwine, O. D.; Shankar, R. B.; Timmers, F. J.; Abboud, K. A. *J. Am. Chem. Soc.* **2007**, *129*, 7065−7076. (b) Noh, S. K.; Lee, M.; Kum, D. H.; Kim, K.; Lyoo, W. S.; Lee, D. H. *J. Polym. Sci., Part A: Polym. Chem.* **2004**, *42*, 1712−1723. (c) Noh, S. K.; Yang, Y.; Lyoo, W. S. *J. Appl. Polym. Sci.* **2003**, *90*, 2469−2474. (d) Sukhova, T. A.; Panin, A. N.; Babkina, O. N.; Bravaya, N. M. *J. Polym. Sci., Part A: Polym. Chem.* **1999**, *37*, 1083−1093. (e) Xu, G. *Macromolecules* **1998**, *31*, 2395−2402. (f) Sernetz, F. G.; Mülhaupt, R.; Amor, F.; Eberle, T.; Okuda, J. *J. Polym. Sci., Part A: Polym. Chem.* **1997**, *35*, 1571−1578. (g) Timmers, F. J. U.S. Patent 5703187, 1997. (h) Sernetz, F. G.; Mülhaupt, R.; Waymouth, R. M. *Macromol. Chem. Phys.* **1996**, *197*, 1071−1083. (i) Stevens, J. C.; Timmers, F. J.; Wilson, D. R.; Schmidt, G. F.; Nickias, P. N.; Rosen, R. K.; Knight, G. W.; Lai, S. Y. *Eur. Pat. Appl.* **1991**, *58*, EP 0 416 815 A2.

(13) (a) Kern, R. J.; Hurst, H. G.; Richard, W. R. *J. Polym. Sci.* **1960**, *45*, 195−204. (b) Overberger, C.; Ang, F.; Mark, H. *J. Polym. Sci.* **1959**, *35*, 381−389. (c) Natta, G.; Pino, P.; Corradini, P.; Danusso, F.; Mantica, E.; Mazzanti, G.; Moraglio, G. *J. Am. Chem. Soc.* **1955**, *77*, 1708−1710.

(14) For examples of anionic isospecific styrene polymerization, see: (a) Makino, T.; Hogen-Esch, T. E. *Macromolecules* **1999**, *32*, 5712−5714. (b) Cazzaniga, L.; Cohen, R. E. *Macromolecules* **1989**, *22*, 4125−4128.

(15) (a) De Carlo, F.; Capacchione, C.; Schiavo, V.; Proto, A. *J. Polym. Sci., Part A: Polym. Chem.* **2006**, *44*, 1486−1491. (b) Beckerle, K.; Manivannan, R.; Spaniol, T. P.; Okuda, J. *Organometallics* **2006**, *25*, 3019−3026. (c) Capacchione, C.; Manivannan, R.; Barone, M.; Beckerle, K.; Centore, R.; Oliva, L.; Proto, A.; Tuzi, A.; Spaniol, T. P.; Okuda, J. *Organometallics* **2005**, *24*, 2971−2982. (d) Capacchione, C.; Proto, A.; Ebeling, H.; Mulhaüpt, R.; Möller, K.; Spaniol, T. P.; Okuda, J. *J. Am. Chem. Soc.* **2003**, *125*, 4964−4965.

(16) (a) Knjazhanski, S. Y.; Cadenas, G.; García, M.; Pérez, C. M.; Nifant'ev, I. E.; Kashulin, I. A.; Ivchenko, P. V.; Lyssenko, K. A. *Organometallics* **2002**, *21*, 3094−3099. (b) Nomura, K.; Komatsu, T.; Imanishi, Y. *Macromolecules* **2000**, *33*, 8122−8124. (c) Kaminsky, W.; Lenk, S.; Scholz, V.; Roesky, H. W.; Herzog, A. *Macromolecules* **1997**, *30*, 7647−7650. (d) Foster, P. F.; Chien, J. C. W.; Rausch, M. D. *Organometallics* **1996**, *15*, 2404−2409. (e) Pellecchia, C.; Longo, P.; Proto, A.; Zambelli, A. *Makromol. Chem., Rapid Commun.* **1992**, *13*, 265−268. (f) Ishihara, N.; Kuramoto, M.; Uoi, M. *Macromolecules* **1988**, *21*, 3356−3360.

(17) (a) Chen, J.; Li, Y.; Wu, J.; Hu, N. *J. Mol. Cat. A: Chem.* **2005**, *232*, 1−7. (b) Kim, Y.; Han, Y.; Hwang, J.; Kim, M. W.; Do, Y. *Organometallics* **2002**, *21*, 1127−1135.

(18) Zambelli, A.; Oliva, L.; Pellecchia, C. *Macromolecules* **1989**, *22*, 2129−2130.

(19) For examples of phenyl ring "back-coordination" to d^0 Ti or Zr, see: (a) Manke, D. R.; Nocera, D. G. *Inorg. Chim. Acta* **2003**, *345*, 235−240. (b) Cotton, F. A.; Murillo, C. A.; Petrukhina, M. A. *J. Organomet. Chem.* **1999**, *573*, 78−86. (c) Warren, T. H.; Schrock, R. R.; Davis, W. M. *Organometallics* **1996**, *15*, 562−569. (d) Bochmann, M.; Lancaster, S. J.; Hursthouse, M. B.; Malik, K. M. A. *Organometallics* **1994**, *13*, 2235−2243. (e) Pellecchia, C.; Grassi, A.; Zambelli, A. *Organometallics* **1994**, *13*, 298−302. (f) Pellecchia, C.; Grassi, A.; Immirzi, A. *J. Am. Chem. Soc.* **1993**, *115*, 1160−1162. (g) Pellecchia, C.; Immirzi, A.; Grassi, A.; Zambelli, A. *Organometallics* **1993**, *12*, 4473−4478. (h) Bochmann, M.; Lancaster, S. J. *Organometallics* **1993**, *12*, 633−640. (i) Jordan, R. F.; LaPointe, R. E.; Bajgur, C. S.; Echols, S. F.; Willett, R. *J. Am. Chem. Soc.* **1987**, *109*, 4111−4113. (j) Stoeckli-Evans, H. *Helv. Chim. Acta* **1974**, *57*, 684−689. (k) Bassi, I. W.; Allegra, G.; Scordamaglia, R.; Chioccola, G. *J. Am. Chem. Soc.* **1971**, *93*, 3787−3788.

(20) For studies of styrene insertion regiochemistry, see: (a) Capacchione, C.; Proto, A.; Ebeling, H.; Mulhaüpt, R.; Möller, K.; Spaniol, T. P.; Okuda, J. *J. Am. Chem. Soc.* **2003**, *125*, 4964−4965. (b) Izzo, L.; Napoli, M.; Oliva, L. *Macromolecules* **2003**, *36*, 9340−9345. (c) Caporaso, L.; Izzo, L.; Zappile, S.; Oliva, L. *Macromolecules* **2000**, *33*, 7275−7282. (d) Pellecchia, C.; Pappalardo, D.; Oliva, L.; Zambelli, A. *J. Am. Chem. Soc.* **1995**, *117*, 6593−6594. (e) Zambelli, A.; Longo, P.; Pellecchia, C.; Grassi, A. *Macromolecules* **1987**, *20*, 2035−2037. (f) Pellecchia, C.; Longo, P.; Grassi, A.; Ammendola, P.; Zambelli, A. *Makromol. Chem., Rapid Commun.* **1987**, *8*, 277−279.

Chart 2

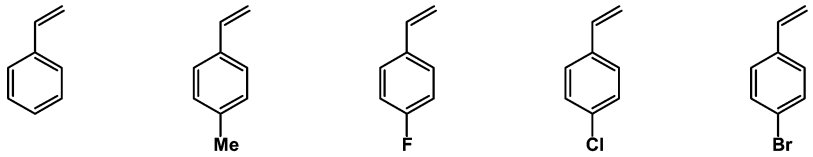

indenyl)[1-Me_2Si(^{t}BuN)][Ti($CH_2Ph)_2$]}$_2$ [**$Ti_2(CH_2Ph)_4$**] was designed, synthesized, characterized, and activated with the cocatalyst/activator $B(C_6F_5)_3$ to probe structural aspects of the proposed mechanism for the observed bimetallic enchainment effects.

Previously, it was reported that a polar solvent can depress bimetallic effects in ethylene copolymerization by weakening/supplanting mechanistically important agostic interactions.[5a,b] In the present study, we carry out detailed ethylene−styrene copolymerizations in the same polar solvent to determine whether such medium effects can weaken/displace the metal-arene interactions. It will be seen that, by manipulating the achievable metal−metal distances, styrenic comonomer substituents (**B**-**F**), and polymerization medium, the observed bimetallic effects can be varied dramatically.

Experimental Section

Materials and Methods. All manipulations of air-sensitive materials were performed with rigorous exclusion of oxygen and moisture in flamed Schlenk-type glassware on a dual-manifold Schlenk line or interfaced to a high-vacuum line (10^{-5} Torr), or in a dinitrogen-filled MBraun and Vacuum Atmospheres glove box with a high capacity recirculator (<1 ppm O_2). Argon (Matheson or Airgas, prepurified) and ethylene (Matheson or Airgas, polymerization grade) were purified by passage through a supported MnO oxygen-removal column and an activated Davison 4A molecular sieve column. Hydrocarbon solvents (toluene and pentane) were dried using an activated alumina column and Q-5 columns according to the method described by Grubbs,[21] and were additionally vacuum transferred from Na/K alloy and stored in Teflon-valve sealed bulbs for polymerization experiments. Ether solvents (THF and Et_2O) were distilled under nitrogen from sodium benzophenone ketyl. The solvent 1,2-difluorobenzene was distilled from CaH_2 and stored over freshly activated Davison 4A molecular sieves. Deuterated solvents were purchased from Cambridge Isotope Laboratories (all ≥99 atom % D). Methylene chloride-d_2 was dried over CaH_2 and vacuum-transferred into J. Young NMR tubes. The solvent for polymer NMR characterization, 1,1,2,2-tetrachloroethane-d_2, was used as received. Other deuterated solvents were distilled from Na/K alloy and stored in vacuum-tight storage tubes over freshly activated Davison 4A molecular sieves. Chlorobenzene, styrene, 4-methylstyrene, 4-fluorostyrene, 4-chlorostyrene, and 4-bromostyrene (Aldrich) were dried sequentially for a week over CaH_2 and then triisobutylaluminum and were freshly vacuum-transferred prior to polymerization experiments. The reagent TMSCl was purchased from Aldrich and redistilled. The reagent $PhCH_2MgCl{\cdot}0.66Et_2O$ was prepared by removing all the volatiles from $PhCH_2MgCl$ (1.0 M in Et_2O) (Aldrich). The reagent (μ-CH_2CH_2-3,3′){(η^5-indenyl)[1-Me_2Si(^{t}BuN)][Ti($NMe_2)_2$]}$_2$ {EBICGC-[Ti($NMe_2)_2$]$_2$; **$Ti_2(NMe_2)_4$**}, and the catalysts **Ti_1**, **Ti_2**, **C1-Ti_2**, **Zr_1**, **Zr_2**, and **C1-Zr_2** were prepared and purified according to literature procedures.[5a,b]

Physical and Analytical Measurements. NMR spectra were recorded on a Varian Innova 400 (FT 400 MHz, ^{1}H; 100 MHz, ^{13}C), Unity- or Mercury-400 (FT, 400 MHz, ^{1}H; 100 MHz, ^{13}C), or Inova-500 (FT, 500 MHz, ^{1}H; 125 MHz, ^{13}C) spectrometer. Chemical shifts (δ) for ^{1}H and ^{13}C spectra were referenced using internal solvent resonances and are reported relative to tetramethylsilane. NMR experiments on air-sensitive samples were conducted in Teflon valve-sealed sample tubes (J. Young). ^{13}C NMR assays of polymer microstructure were conducted in 1,1,2,2-tetrachloroethane-d_2 containing 0.05 M Cr(acac)$_3$ (as a relaxation reagent) at 130 °C. Resonances were assigned according to the literature for polystyrene and ethylene−styrene copolymers. Elemental analyses were performed by Midwest Microlabs, LLC, Indianapolis, Indiana.

Gel permeation chromatographic (GPC) analysis was carried out on a Waters Alliance GPCV 2000 high-temperature instrument equipped with three Polymer Laboratories 10 μm mixed B columns (three columns: Waters Styragel HT 6E, HT 4, HT 2) operating at 150 °C and a refractive index detector. A flow rate of 1.0 mL/min was used, and HPLC grade 1,2,4-trichlorobenzene was employed as the eluent. Typically, ca. 5 mg of the sample was dissolved in 7.0 mL of TCB. The hot solutions were filtered using a 0.5 μm stainless steel filter. A polystyrene relative calibration was carried out using narrow molecular weight distribution polystyrene standards from Polymer Laboratories with Ionol (4-(2,6,6-trimethyl-2-cyclohexen-1-yl)-3-buten-2-ol) added as the flow marker.[22] Alternatively, GPC measurements were performed on a Polymer Laboratories PL-GPC 220 instrument using 1,2,4-trichlorobenzene solvent (stabilized with 125 ppm BHT) at 150 °C. A set of three PLgel 10 μm mixed columns was used. Samples were prepared at 160 °C. Molecular weights were determined by GPC using narrow polystyrene standards and are uncorrected.

Polymer glass transition temperatures and melting temperatures were measured on a TA Instruments 2920 Modulated Differential Scanning Calorimeter. Typically, ca. 10 mg samples were examined, and a ramp rate of 10 °C/min was used to measure the polymer glass transition points and melting points. To erase thermal history effects, all samples were run through at least two melt−freeze cycles. The data from the second melt−freeze cycle are presented here.

Styrene Homopolymerization Experiments in Toluene. In the glovebox, a 250 mL round-bottom three-neck Morton flask, which had been dried at 160 °C overnight and equipped with a large magnetic stirring bar and a thermocouple probe, was charged with 25 mL of dry toluene and 5 mL of dry styrene. The flask was then attached to a high-vacuum line (10^{-5} Torr) and equilibrated at the desired reaction temperature using an external bath. The catalytically active species was freshly generated in 1.5 mL of dry 1,2-difluorobezene in the nitrogen-filled glovebox. Under 1.0 atm of rigorously purified argon (pressure control using a mercury bubbler), the catalyst solution was quickly injected into the rapidly stirred flask using a gastight syringe equipped with a flattened spraying needle. After a measured time interval, the polymerization was quenched by the addition of 5 mL of methanol, and the reaction mixture was then poured into 800 mL of methanol. The polymer was allowed to fully precipitate overnight and then collected by filtration, washed with fresh methanol, and dried on a high-vacuum line overnight at 80 °C to constant weight.

Ethylene Copolymerization Experiments in Toluene. In the glovebox, a 250 mL round-bottom three-neck Morton flask, which had been dried at 160 °C overnight and equipped with a large magnetic stirring bar and a thermocouple probe, was charged with 50 mL of dry

(21) Pangborn, A. B.; Giardello, M. A.; Grubbs, R. H.; Rosen, R. K.; Timmers, F. J. *Organometallics* **1996**, *15*, 1518−1520.

toluene and 10 mL of dry styrene. The flask was then attached to a high-vacuum line (10^{-5} Torr), freeze−pump−thaw degassed, presaturated with 1.0 atm (pressure control using a mercury bubbler) of rigorously purified ethylene, and equilibrated at the desired reaction temperature using an external bath. The catalytically active species was freshly generated in 1.5 mL of dry 1,2-difluorobezene in the nitrogen-filled glovebox. The catalyst solution was then quickly injected into the rapidly stirred flask using a gastight syringe equipped with a flattened spraying needle. After a measured time interval, the polymerization was quenched by the addition of 5 mL of methanol, and the reaction mixture was then poured into 800 mL of methanol. The polymer was allowed to fully precipitate overnight and then collected by filtration, washed with fresh methanol, and dried on a high vacuum line overnight at 80 °C to constant weight.

Ethylene Copolymerization Experiments in Chlorobenzene. In the glovebox, a 250 mL round-bottom three-neck Morton flask, which had been dried at 160 °C overnight and equipped with a large magnetic stirring bar and a thermocouple probe, was charged with 10 mL of dry styrene. The flask was then attached to a high-vacuum line (10^{-5} Torr), freeze−pump−thaw degassed, and then 50 mL of chlorobenzene was vacuum transferred in. The flask was presaturated with 1.0 atm (pressure control using a mercury bubbler) of rigorously purified ethylene and equilibrated at the desired reaction temperature using an external bath. The catalytically active species was freshly generated in 1.5 mL of dry 1,2-difluorobezene in the nitrogen-filled glovebox. The catalyst solution was then quickly injected into the rapidly stirred flask using a gastight syringe equipped with a flattened spraying needle. After a measured time interval, the polymerization was quenched by the addition of 5 mL of methanol, and the reaction mixture was then poured into 800 mL of methanol. The polymer was allowed to fully precipitate overnight and then collected by filtration, washed with fresh methanol, and dried on a high-vacuum line overnight at 80 °C to constant weight.

Determination of Comonomer Content by ^{1}H NMR. The solvent 1,1,2,2-tetrachloroethane-d_2 ($C_2D_2Cl_4$) was used as the deuterated solvent for polymer NMR analysis because its NMR spectral features do not overlap with any of the polymer resonances. Delay times of 20 s were used to ensure the accuracy of NMR peak integration. The comonomer contents were calculated based on the integral of the aromatic region (A_{aromatic}) and the aliphatic region ($A_{\text{aliphatic}}$) according to the following equations:

$$\text{poly(ethylene}-co-\text{styrene)}\ S\% = \frac{4A_{\text{aromatic}}}{A_{\text{aromatic}} + 5A_{\text{aliphatic}}}$$

$$\text{poly(ethylene}-co-\text{4-halostyrene)}\ S\% = \frac{4A_{\text{aromatic}}}{A_{\text{aromatic}} + 4A_{\text{aliphatic}}}$$

$$\text{poly(ethylene}-co-\text{4-methylstyrene)}\ S\% = \frac{2A_{\text{aromatic}}}{2A_{\text{aliphatic}} - A_{\text{aromatic}}}$$

Solvent Fractionation of Ethylene-*co*-styrene and Polystyrene Mixtures. A known amount of polymer mixture was loaded into a cellulose fiber thimble placed inside a Soxhlet extractor. Methyl ethyl ketone (MEK) was used as the solvent to extract the polystyrene. After 24 h of refluxing, the remaining insoluble copolymer was carefully collected and dried on a high vacuum line overnight at 80 °C to constant weight.

X-Ray Crystal Structure Determination of $Ti_2(CH_2Ph)_4$. Crystals of the title complex suitable for X-ray diffraction were obtained by slow diffusion of pentane into a saturated toluene solution at room temperature. Inside the glovebox, the crystals were placed on a glass slide and covered with dry Infineum V8512 oil. The crystals were then removed from the box, and a suitable crystal was selected under a microscope using plane-polarized light. The crystal was mounted on a glass fiber and transferred to a Bruker SMART 1000 CCD area detector diffractometer in a nitrogen cold stream at 153 (2) K. Diffraction data were obtained with a fine focus, sealed tube Mo Kα radiation source ($\lambda = 0.71073$ Å) and a graphite monochromator. Twenty frames (20 s exposures, 0.3° slices) were collected in three areas of space to determine the orientation matrix. The parameters for data collection were determined by the peak intensities and widths from the 60 frames used to determine the orientation matrix. The faces of the crystal were then indexed and data collection was begun. After data collection, the frames were integrated, the initial crystal structure was solved by direct methods, the structure solution was refined through successive least-squares cycles and subjected to a face-indexed absorption correction. Crystal data, data collection, and refinement parameters are summarized in Table 4 and in the Crystallographic Information File (CIF, see Supporting Information).

Synthesis of Bimetallic Metallocene Complex Ti_2Cl_4. The reagent **$Ti_2(NMe_2)_4$** (500 mg, 0.638 mmol) was partially dissolved in 75 mL of dry toluene in a 100 mL Schlenk flask and the solution was cooled to −78 °C. Next, Me_3SiCl (3.0 mL, 23.64 mmol) was added dropwise by syringe with stirring. The solution was then allowed to slowly warm to room temperature and to stir for 48 h. Large quantities of wine-red solid precipitated, which was separated by filtration, washed with fresh pentane, and subsequently dried on the high-vacuum line. Yield: 370 mg (77%). This product was used for the next reaction without further purification. ^{1}H NMR (C_6D_6, 23 °C, 499.748 MHz): δ 7.58 (d, 2H, $^3J_{H-H} = 8.5$ Hz, Ind, C_6H_4), 7.36 (d, 2H, $^3J_{H-H} = 8.5$ Hz, Ind, C_6H_4), 7.04 (t, 2H, $^3J_{H-H} = 7.5$ Hz, Ind, C_6H_4), 6.94 (t, 2H, $^3J_{H-H} = 8.0$ Hz, Ind, C_6H_4), 6.25 (s, 2H, Ind, C_5H), 3.59 (dd, 2H, $^2J_{H-H} = 14.5$ Hz, $^3J_{H-H} = 8.5$ Hz, CH_2CH_2), 3.25 (dd, 2H, $^2J_{H-H} = 14.0$ Hz, $^3J_{H-H} = 8.0$ Hz, CH_2CH_2), 1.31 (s, 18H, $NCMe_3$), 0.53 (s, 6H, $SiMe_2$), 0.28 (s, 6H, $SiMe_2$). Anal. Calcd for $C_{32}H_{44}N_2Si_2Cl_4Ti_2$: C, 51.21; H, 5.92; N, 3.73. Found: C, 51.14; H, 5.84; N, 3.98.

Synthesis of Bimetallic Metallocene Complex $Ti_2(CH_2Ph)_4$. Ti_2Cl_4 (150 mg, 0.200 mmol) was suspended in 75 mL of dry toluene in a 100 mL Schlenk flask, and after the mixture was cooled to −78 °C, $PhCH_2MgCl{\cdot}0.66Et_2O$ (153 mg, 0.764 mmol) dissolved in 10 mL of dry toluene was added dropwise by syringe with stirring. The reaction mixture was then allowed to warm to room temperature and stirring continued for 24 h. Next, the $MgCl_2$ precipitate was filtered off, and the red filtrate was condensed to saturation and slowly cooled to −40 °C to afford red crystals, which were isolated by filtration, washed with cold pentane twice, and subsequently dried on the high-vacuum line. Yield: 80 mg (41%). Spectropic and analytical data are: ^{1}H NMR (C_6D_6, 23 °C, 499.748 MHz): δ 7.66 (d, 2H, $^3J_{H-H} = 8.5$ Hz, Ind, C_6H_4), 7.54 (d, 2H, $^3J_{H-H} = 8.5$ Hz, Ind, C_6H_4), 7.40−6.70 (m, *Ind* + $TiCH_2Ph$), 5.75 (s, 2H, Ind, C_5H), 3.49 (dd, 2H, $^2J_{H-H} = 14.0$ Hz, $^3J_{H-H} = 6.2$ Hz, CH_2CH_2), 3.34 (dd, 2H, $^2J_{H-H} = 14.0$ Hz, $^3J_{H-H} = 6.2$ Hz, CH_2CH_2),, 3.18 (d, 2H, $^2J_{H-H} = 10.0$ Hz, $TiCH_2Ph$), 2.05 (d, 2H, $^2J_{H-H} = 10.0$ Hz, $TiCH_2Ph$), 1.83 (d, 2H, $^2J_{H-H} = 10.5$ Hz, $TiCH_2Ph$), 1.49 (s, 18H, $NCMe_3$), 0.61 (s, 6H, $SiMe_2$), 0.27 (s, 6H, $SiMe_2$), 0.20 (d, 2H, $^2J_{H-H} = 10.0$ Hz, $TiCH_2Ph$). ^{1}H NMR (CD_2Cl_2, 23 °C, 499.748 MHz): δ 7.83 (d, 2H, $^3J_{H-H} = 8.5$ Hz, Ind, C_6H_4), 7.60 (d, 2H, $^3J_{H-H} = 8.0$ Hz, Ind, C_6H_4), 7.52 (t, 2H, $^3J_{H-H} = 7.0$ Hz, Ind, C_6H_4), 7.18 (t, 2H, $^3J_{H-H} = 7.5$ Hz, Ind, C_6H_4), 7.025 (t, 4H, $^3J_{H-H} = 7.8$ Hz, *m*-Ph), 7.022 (t, 4H, $^3J_{H-H} = 7.5$ Hz, *m*-Ph), 6.79 (t, 4H, $^3J_{H-H} = 7.5$ Hz, *p*-Ph), 6.76 (t, 4H, $^3J_{H-H} = 7.8$ Hz, *p*-Ph), 6.71 (d, 2H, $^3J_{H-H} = 7.0$ Hz, *o*-Ph), 6.62 (d, 2H, $^3J_{H-H} = 7.0$ Hz, *o*-Ph), 5.50 (s, 2H, Ind, C_5H), 3.33 (dd, 2H, $^2J_{H-H} = 8.0$ Hz, $^3J_{H-H} = 3.5$ Hz, CH_2CH_2), 3.26 (dd, 2H, $^2J_{H-H} = 7.5$ Hz, $^3J_{H-H} = 4.0$ Hz, CH_2CH_2), 2.80 (d, 2H, $^2J_{H-H} = 10.5$ Hz, $TiCH_2Ph$), 1.75 (d, 2H, $^2J_{H-H} = 10.0$ Hz, $TiCH_2Ph$), 1.64 (2H, $TiCH_2Ph$, overlapping with $NCMe_3$), 1.62 (s, 18H, $NCMe_3$), 0.80 (s, 6H, $SiMe_2$), 0.18 (s, 6H, $SiMe_2$), −0.23 (d, 2H, $^2J_{H-H} = 10.5$ Hz, $TiCH_2Ph$). ^{13}C{^{1}H} NMR (CD_2Cl_2, 23 °C, 125.674 MHz): δ 150.09 (*ipso*-$TiCH_2Ph$), 146.58 (*ipso*-$TiCH_2Ph$), 134.56 (*Ind*), 133.25 (*Ind*), 131.27 (*Ind*), 129.51 (*Ind*), 129.02 (*ortho*-$TiCH_2Ph$), 128.70 (*ortho*-$TiCH_2Ph$), 128.27 (*meta*-$TiCH_2Ph$), 128.11 (*Ind*), 127.03 (*meta*-$TiCH_2Ph$), 126.72 (*Ind*), 125.90 (*Ind*), 123.99 (*Ind*), 122.76 (*para*-$TiCH_2Ph$), 122.06 (*para*-$TiCH_2Ph$), 94.34 (*Ind*), 84.90 ($TiCH_2Ph$), 80.23

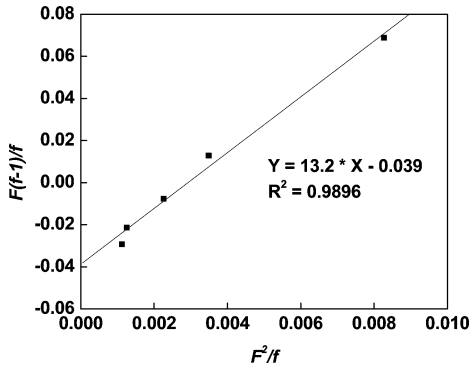

Figure 1. Fineman-Ross plot for $\mathbf{Ti_2}$ + $\mathbf{B_1}$-mediated ethylene−styrene copolymerization, F = ethylene/styrene feed ratio, f = ethylene content in copolymer in mol %/styrene content in copolymer in mol %.

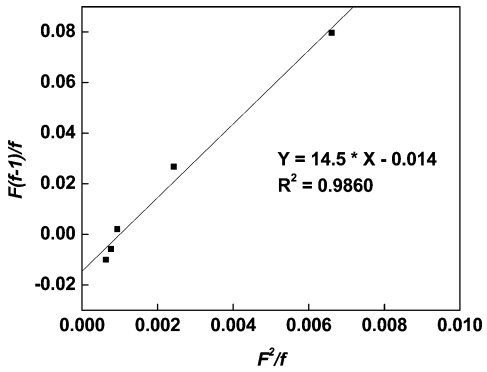

Figure 2. Fineman-Ross plot for $\mathbf{Ti_1}$ + $\mathbf{B_1}$-mediated ethylene−styrene copolymerization, F = ethylene/styrene feed ratio, f = ethylene content in copolymer in mol %/styrene content in copolymer in mol %.

(TiCH_2Ph), 61.28 (NCMe_3), 34.46 (NCMe_3), 30.12 (CH_2CH_2), 4.46 (SiMe_2), 1.26 (SiMe_2). Anal. Calcd for $C_{60}H_{72}N_2Si_2Ti_2$: C, 74.04; H, 7.47; N, 2.88. Found: C, 74.80; H, 7.47; N, 2.90.

In Situ NMR Study of the Bimetallic Metallocene Ion Pair $[\mathbf{Ti_2(CH_2Ph)_2}]^{2+}[\mathbf{PhCH_2B(C_6F_5)_3}^-]_2$. In the glove box, $\mathbf{Ti_2(CH_2Ph)_4}$ and $B(C_6F_5)_3$ in a 1:2 molar ratio were loaded into a J. Young NMR tube. The sealed tube was then removed from the glovebox, attached to the vacuum line, and cooled to −78 °C, and CD_2Cl_2 was immediately transferred in. The sample was shaken vigorously and transferred directly to the NMR spectrometer. Upon activation, the solution color changed from red to dark brown. ^{1}H NMR (C_6D_6, 23 °C, 499.748 MHz): δ 7.60−6.20 (m, Ind + Ti^+CH_2Ph + B^-CH_2Ph), 5.68 (s, 2H, Ind, C_5H), 3.62 (br, 4H, B^-CH_2Ph), 2.91 (d, 2H, $^2J_{H-H}$ = 8.5 Hz, Ti^+CH_2Ph), 2.43 (d, 2H, $^2J_{H-H}$ = 7.5 Hz, Ti^+CH_2Ph), 1.05 (s, 18H, NCMe_3), 0.26 (s, 6H, SiMe_2), 0.10 (s, 6H, SiMe_2).

Results

The goal of this study was to investigate the scope, kinetics, and mechanism of bimetallic enchainment cooperative effects in styrene homopolymerization and ethylene−styrene copolymerizations. Previously, we briefly communicated evidence for such bimetallic effects in the case of $\mathbf{Ti_2}$, manifested by significantly greater activity in styrene homopolymerization and enhanced comonomer incorporation in ethylene−styrene copolymerization. In this contribution, we extend the study to include organozirconium catalysts and broaden the copolymerization scope to include a variety of informative styrenic comonomers. We also design, synthesize, and characterize a bimetallic model compound to probe the coordination mode of inserted styrene to the coordinatively open and highly electrophilic single-site catalytic center. After a brief discussion of the kinetics of $\mathbf{Ti_2}$ and $\mathbf{Ti_1}$-mediated ethylene−styrene copolymerization, we discuss the effects of styrene substituents on the comonomer incorporation difference between $\mathbf{Ti_2}$ and $\mathbf{Ti_1}$. Next, styrene homopolymerization will be addressed in terms of polymerization activity and insertion regiochemistry. Finally, the effect of polar solvation on the bimetallic cooperative effects is discussed.

Scheme 2. Propagation Patterns in Ethylene−Styrene Copolymerization for a First-Order Markovian Statistical Model

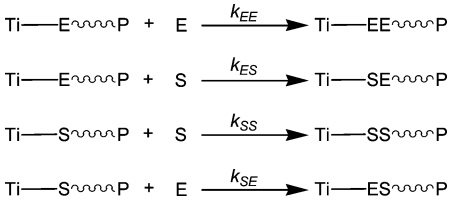

I. KineticAnalyses of Ethylene−Styrene Copolymerization Mediated by $\mathbf{Ti_2}$ + $\mathbf{B_1}$ and $\mathbf{Ti_1}$ + $\mathbf{B_1}$. Previously, we reported that under identical copolymerization conditions, the catalytic system $\mathbf{Ti_2}$ + $\mathbf{B_1}$ incorporates significantly more styrene into the polyethylene backbone than does $\mathbf{Ti_1}$ + $\mathbf{B_1}$. To understand this bimetallic effect on the selectivity of monomer enchainment, kinetic analyses were carried out to determine the reactivity ratios for both monomers. A series of ethylene−styrene copolymerizations were carried out with increasing styrene: ethylene feed ratios for both $\mathbf{Ti_2}$ + $\mathbf{B_1}$ and $\mathbf{Ti_1}$ + $\mathbf{B_1}$-mediated copolymerizations. All the copolymerization experiments were terminated at low styrene conversions (<10%) to ensure a constant feed ratio.

First-Order Markovian Analysis. In a first-order Markovian model for ethylene−styrene copolymerization statistics, which takes into account only the influence of the last inserted monomer during chain propagation,[23a] the reactivity ratios r_E and r_S are defined as the ratios of homopropagation rate constants to crosspropagation rate constants of ethylene and styrene, respectively ($r_E = k_{EE}/k_{ES}$, $r_S = k_{SS}/k_{SE}$, Scheme 2). With styrene content in the monomer feed and in the copolymer known, the reactivity ratios can be obtained from Fineman-Ross plots (Figures 1 and 2).[23a] For $\mathbf{Ti_2}$ + $\mathbf{B_1}$-mediated ethylene−styrene copolymerization, the slope and the intercept of the Fineman-Ross plot yield the values $r_E = 13.2 \pm 0.8$ and $r_S = 0.039 \pm 0.003$, respectively, whereas for $\mathbf{Ti_1}$ + $\mathbf{B_1}$, the Fineman-Ross plot gives the values $r_E = 14.5 \pm 1.0$ and $r_S = 0.014 \pm 0.003$. It can be seen that $\mathbf{Ti_2}$ + $\mathbf{B_1}$ possesses a significantly larger r_S and slightly smaller r_E than $\mathbf{Ti_1}$ + $\mathbf{B_1}$, in agreement with the NMR analytical observations that $\mathbf{Ti_2}$ always incorporates more styrene than $\mathbf{Ti_1}$ under identical reaction conditions.

Second-Order Markovian Analysis. The second-order Markovian assumption takes into account the influence of the second-to-the-last inserted monomer unit on incoming monomer enchainment selectivity.[23a] As shown in Scheme 3, when the last inserted monomer is ethylene, four different propagation equations can be written (eqs 1−4). Dividing eq 1 by eq 2 and eq 3 by eq 4 yields eqs 5 and 6, respectively, where X_E is the ethylene:styrene feed ratio. Two reactivity ratios are defined to

(22) Protivova, J.; Pospisil, J.; Zikmund, L. *J. Polym. Sci. Polym Symposia* **1973**, *40*, 233−243.
(23) (a) Fink, G.; Richter, W. J. In *Polymer Handbook*, 4th ed.; Brandup, J., Immergut, E. H., Grulke, E. A., Eds.; John Wiley & Sons: New York, 1999; Vol. II, pp 329−337. (b) Oliva, L.; Longo, P.; Izzo, L.; Di Serio, M. *Macromolecules* **1997**, *30*, 5616−5619.

Scheme 3. Propagation Patterns in Ethylene−Styrene Copolymerizations for a Second-Order Markovian Statistical Model

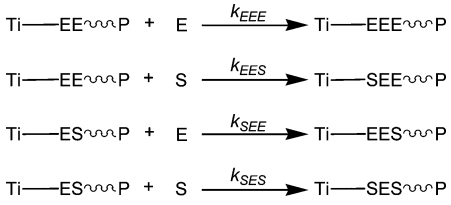

quantify the preference of ethylene over styrene to be inserted into the Ti−polymeryl bond when the second-to-the-last inserted monomer is ethylene (r_E) or styrene (r'_E).[23b] If r_E is inequivalent to r'_E, then the penultimate unit specifically exerts an effect on the incoming monomer enchainment selectivity.

$$\frac{d[EEE]}{dt} = k_{EEE}[Ti{-}EE{-}P]\,[E] \quad (1)$$

$$\frac{d[EES]}{dt} = k_{EES}[Ti{-}EE{-}P]\,[S] \quad (2)$$

$$\frac{d[SEE]}{dt} = k_{SEE}[Ti{-}ES{-}P]\,[E] \quad (3)$$

$$\frac{d[SES]}{dt} = k_{SES}[Ti{-}ES{-}P]\,[S] \quad (4)$$

$$\frac{[EEE]}{[EES]} = \frac{k_{EEE}\,[E]}{k_{EES}\,[S]} = r_E\,X_E \quad (5)$$

$$\frac{[SEE]}{[SES]} = \frac{k_{SEE}\,[E]}{k_{SES}\,[S]} = r'_E\,X_E \quad (6)$$

Figure 3 shows a typical ^{13}C NMR spectrum of an ethylene−styrene copolymer and its assignments (see more below), from which the triad distribution can be extracted (eqs 7−9). As illustrated in Figure 4, for $\mathbf{Ti_2} + \mathbf{B_1}$-mediated ethylene−styrene copolymerization, plotting [EEE]/[EES] and [SEE]/[SES] vs X_E yields straight lines, the slopes of which afford the reactivity ratios defined above (eqs 7 and 8). The fact that r_E

$$[EEE] \propto 0.5(S_{\gamma+\gamma+} - 0.5S_{\beta\gamma+}) \quad (7)$$

$$[SES] \propto S_{\beta\beta} \quad (8)$$

$$[SEE] = [EES] \propto 0.5S_{\beta\gamma+} \quad (9)$$

is larger than r'_E ($r_E = 7.79 \pm 1.02 > r'_E = 3.26 \pm 0.11$) indicates that the aforementioned bimetallic catalyst $\mathbf{Ti_2}$-mediated ethylene−styrene copolymerization follows second-order Markovian statistics (penultimate model), and more interestingly, when the second-to-the-last inserted monomer is styrene and the last inserted one is ethylene, the incoming styrene is preferred over ethylene for insertion into the Ti−polymeryl bond, thereby generating SES triads. This alternating copolymerization trend is also evidenced by the product of the two reactivity ratios defined above by the first-order Markovian statistics ($r_E \times r_S = 0.51$).

For $\mathbf{Ti_1} + \mathbf{B_1}$ mediated ethylene−styrene copolymerization, reactivity ratios can also be obtained by plotting [EEE]/[EES] and [SEE]/[SES] vs X_E (Figure 5). Again, $r_E = 13.49 \pm 0.78$ is larger than $r'_E = 6.45 \pm 0.14$, suggesting that monometallic catalyst $\mathbf{Ti_1}$-mediated ethylene−styrene copolymerization follows second-order Markovian statistics as well. In addition, the values of both reactivity ratios for $\mathbf{Ti_2}$ are invariably smaller than the corresponding ones for $\mathbf{Ti_1}$, demonstrating that $\mathbf{Ti_2}$ favors styrene insertion more than $\mathbf{Ti_1}$, or in other words, $\mathbf{Ti_1}$ favors ethylene insertion more than $\mathbf{Ti_2}$, which is in agreement with the observed bimetallic enchainment selectivity effects that under identical ethylene−styrene copolymerization conditions, bimetallic catalyst $\mathbf{Ti_2}$ incorporates styrene more efficiently than does monometallic catalyst $\mathbf{Ti_1}$.

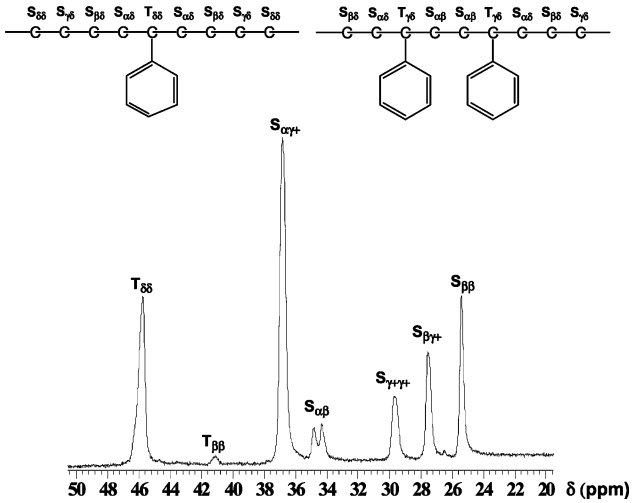

Figure 3. ^{13}C NMR spectrum (100 MHz, $C_2D_2Cl_4$, 130 °C) of poly(ethylene-*co*-styrene) showing spectral assignments in the backbone region.

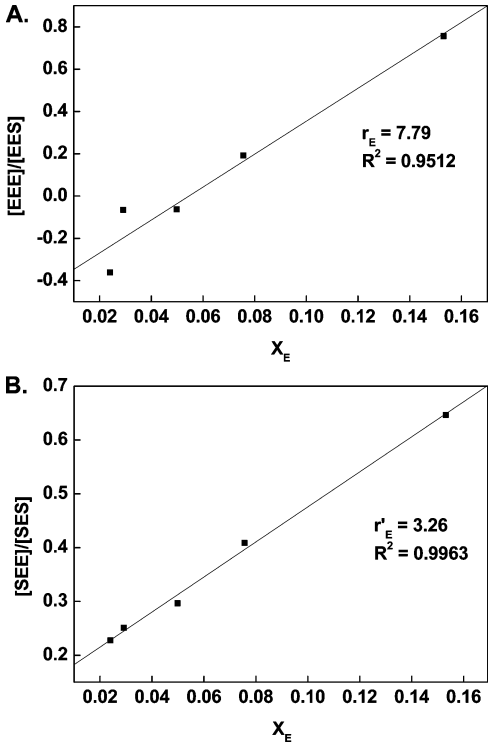

Figure 4. Triad distribution analysis plots for $\mathbf{Ti_2} + \mathbf{B_1}$-mediated ethylene−styrene copolymerization.

II. Copolymerization of Ethylene and Styrenic Comonomers. Previously, we communicated that under identical copolymerization conditions, $\mathbf{Ti_2}$ incorporates significantly more styrene than does $\mathbf{Ti_1}$ in ethylene−styrene copolymerizations. To test the generality of this observed bimetallic effect, a variety of substituted styrenic comonomers with either electron-donating

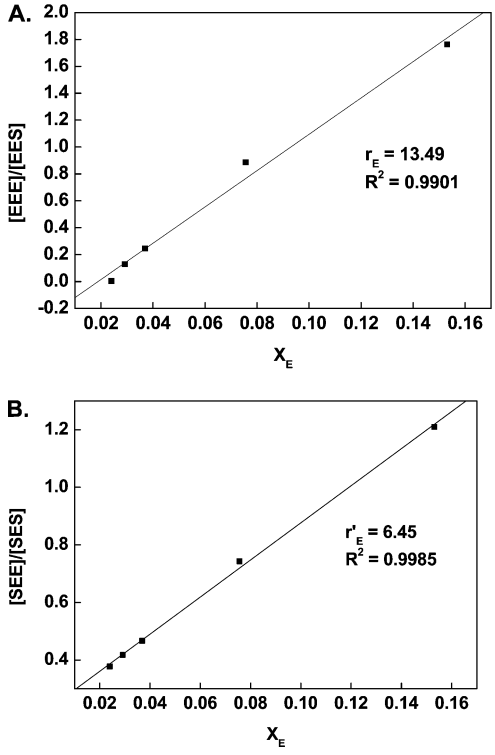

Figure 5. Triad distribution analysis plots for $\mathbf{Ti_1} + \mathbf{B_1}$-mediated ethylene−styrene copolymerization.

or electron-withdrawing substituents at the *para* positions were examined in copolymerization experiments with ethylene and the aforementioned organotitanium catalysts. For all of these styrenic comonomers, it will be seen that the bimetallic catalysts exhibit significantly enhanced comonomer enchainment selectivity versus the monometallic analogue under identical reaction conditions.

Copolymerization of Ethylene and Styrene. Figure 6 shows ^{13}C NMR spectra of the poly(ethylene-*co*-styrene) samples of Table 1, entries 1−3, and assignments made according to literature.[10] The resonances at $\delta = 34.4$ and 34.9 ppm are attributed to $S_{\alpha\beta}$, which represents either a tail-to-tail coupled styrene dyad or an ethylene unit bridged head-to-head coupled styrene dyad. Other polymer resonances centered at $\delta = 25.5$, 27.7, 29.8, 36.9, and 46.0 ppm in the aliphatic region can be assigned to $S_{\beta\beta}$, $S_{\beta\gamma+}$, $S_{\gamma+\gamma+}$, $S_{\alpha\gamma+}$, and $T_{\delta+\delta+}$, respectively, corresponding to SES, SEE, SEE$_n$S, SES + SEE, and E$_n$SE$_n$ ($n \geq 1$) sequences, respectively.[10g] The signals observed at $\delta = 146.4$ and 125.7 ppm in the aromatic region are assigned to the *ipso* carbon and *para* carbon of the phenyl ring attached to the copolymer backbone, respectively.

Regarding nuclearity effects, it is found that under strictly identical copolymerization conditions the $\mathbf{Ti_2} + \mathbf{B_1}$ combination incorporates 15.4% more styrene than the mononuclear analogue $\mathbf{Ti_1} + \mathbf{B_1}$ (Table 1, entry 2 versus entry 3). To further explore the correlation between catalyst structure and polymerization behavior, methylene-bridged **C1-Ti$_2$** was also employed in catalytic studies. It can be seen from entry 1 versus entry 2 in Table 1 that $\mathbf{C1\text{-}Ti_2} + \mathbf{B_1}$ incorporates 14.9% more styrene than does $\mathbf{Ti_2} + \mathbf{B_1}$, presumably due to the enhanced cooperative effects arising from the diminished achievable Ti−Ti distance (see more below).

All of the present ethylene−styrene copolymers are amorphous and exhibit a single glass transition temperature (T_g), suggesting the resultant copolymers have approximately homogeneous styrene distributions. Moreover, it is found that T_g increases from 5.8 to 16.6 °C and then to 22.3 °C as the styrene incorporation level increases from 28.0 to 32.3 mol % and then to 37.1 mol %, in agreement with reported T_g values for copolymers with similar styrene contents.[8c]

Copolymerization of Ethylene and 4-Methylstyrene. The ^{13}C NMR spectra (Figure 7) of the ethylene + 4-methylstyrene copolymers share an almost identical pattern to the ethylene−styrene copolymers in the aliphatic region except for the additional resonance at $\delta = 20.9$ ppm, which can be assigned to the phenyl ring methyl substituent. In the aromatic region, the chemical shifts of the *ipso* carbon and *para* carbon are displaced to $\delta = 143.4$ and 134.7 ppm, respectively. As for the comonomer incorporation level, ^{1}H NMR spectra show that $\mathbf{Ti_2} + \mathbf{B_1}$ enchains 29.9 mol % 4-methylstyrene, which is 28.9% more than does $\mathbf{Ti_1} + \mathbf{B_1}$ (23.2 mol %), and the copolymer T_g also increases from 8.0 to 19.0 °C.

Copolymerization of Ethylene and 4-Fluorostyrene. Figure 8 shows the ^{13}C NMR spectra of representative ethylene + 4-fluorostyrene copolymers. Compared to the ethylene−styrene copolymers, the methylene and ethylene region exhibits an almost identical pattern. In the aromatic region, the *ispo* carbon shifts to $\delta = 142.1$ ppm. The phenyl ring *para* carbon appears as a doublet centered at $\delta = 161.4$ ppm, due to the coupling to the fluoro substituent ($^1J_{C-F} = 243.4$ Hz). As for bimetallic effects in terms of comonomer incorporation level, the ^{1}H NMR

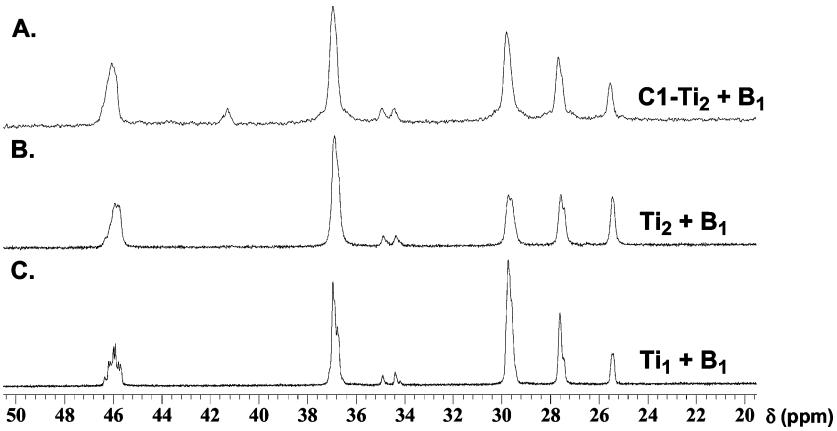

Figure 6. ^{13}C NMR spectra (100 MHz, $C_2D_2Cl_4$, 130 °C) of the poly(ethylene-*co*-styrene) samples from Table 1, entries 1−3 in which catalyst nuclearity and connectivity is varied.

Table 1. Ethylene−Styrene Copolymerization Results for Catalysts $\mathbf{Ti_2}$ and $\mathbf{Ti_1}$ with Cocatalyst $\mathbf{B_1}$[a]

entry	catalyst	comonomer	comonomer concentration (M)	activity[b] (× 10⁶)	T_g[c] (°C)	T_m[c] (°C)	M_w[d] (× 10⁵)	M_w/M_n[d]	comonomer%[e] (mol %)
1	**C1−Ti₂**	**B**	1.45	3.7	22.3	n. o.[f]	10.34	2.2	37.1
2	**Ti₂**	**B**	1.45	5.8	21.7	n. o.	3.67	2.1	32.3
3	**Ti₁**	**B**	1.45	2.2	5.8	n. o.	0.76	1.4	28.0
4	**Ti₂**	**C**	1.26	28.8	19.0	n. o.	1.23	3.3	29.9
5	**Ti₁**	**C**	1.26	24.7	8.0	n. o.	2.14	1.2	23.2
6	**Ti₂**	**D**	1.40	5.9	47.2	n. o.	2.26	1.7	29.8
7	**Ti₁**	**D**	1.40	13.1	44.8	n. o.	3.21	2.1	20.5
8	**Ti₂**	**E**	1.39	3.1	52.7	n. o.	8.55	1.7	20.9
9	**Ti₁**	**E**	1.39	3.1	43.1	n. o.	0.77	1.9	14.8
10	**Ti₂**	**F**	1.27	5.2	48.4	n. o.	6.65	1.7	16.9
11	**Ti₁**	**F**	1.27	4.4	36.0	n. o.	1.50	4.0	12.9

[a] [Ti] = 10 μmol + [B] = 10 μmol at 20 °C, under 1.0 atm ethylene pressure. [b] Units: g polymer/(mol Ti·atm ethylene·h). [c] By DSC. [d] By GPC relative to polystyrene standards. [e] Calculated from ^{1}H NMR. [f] Not observed.

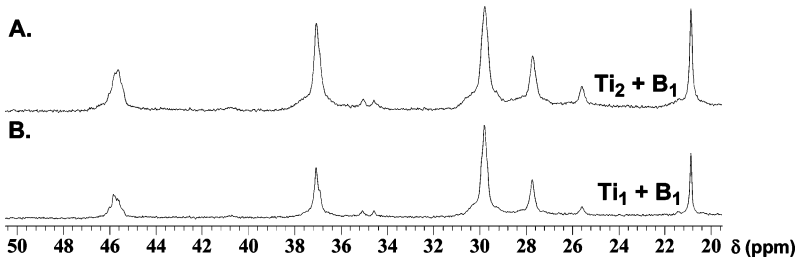

Figure 7. ^{13}C NMR spectra (100 MHz, $C_2D_2Cl_4$, 130 °C) of the poly(ethylene-*co*-4-methylstyrene) samples from Table 1, entries 4−5 in which catalyst nuclearity is varied.

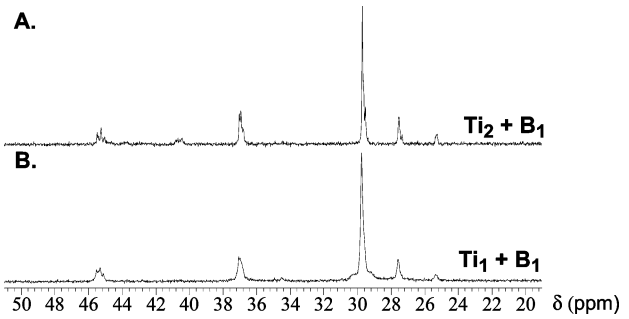

Figure 8. ^{13}C NMR spectra (100 MHz, $C_2D_2Cl_4$, 130 °C) of the poly(ethylene-*co*-4-fluorostyrene) samples from Table 1, entries 6−7, in which the catalyst nuclearity is varied.

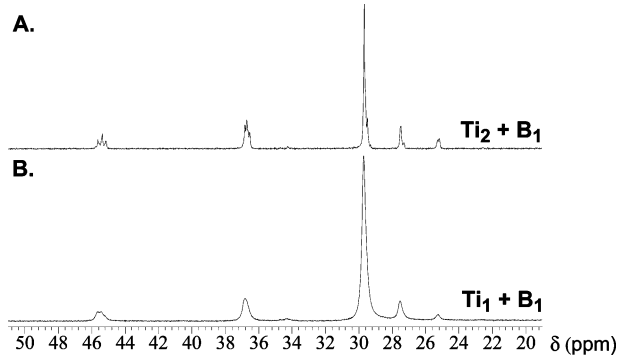

Figure 9. ^{13}C NMR spectra (100 MHz, $C_2D_2Cl_4$, 130 °C) of the poly(ethylene-*co*-4-chlorostyrene) samples from Table 1, entries 8−9, in which the catalyst nuclearity is varied.

data reveal that $\mathbf{Ti_2} + \mathbf{B_1}$ enchains 45.4% more 4-fluorostyrene than does $\mathbf{Ti_1} + \mathbf{B_1}$ (29.8 vs 20.5 mol %). As a result, the copolymer T_g also increases from 44.8 to 47.2 °C.

Copolymerization of Ethylene and 4-Chlorostyrene. The ^{13}C NMR spectra (Figure 9) of the ethylene + 4-chlorostyrene copolymers also share an almost identical pattern to the ethylene−styrene copolymers in the aliphatic region. In the aromatic region, the chemical shifts of the *ipso* and *para* carbons are displaced to δ = 145.0 and 131.5 ppm, respectively. Concerning the comonomer enchainment level, ^{1}H NMR spectra indicate that $\mathbf{Ti_2} + \mathbf{B_1}$ enchains 20.9 mol % 4-chlorostyrene, which is 41.2% greater than does $\mathbf{Ti_1} + \mathbf{B_1}$ (14.8 mol %). As a result, the T_g of the copolymers also increases from 43.1 to 52.7 °C.

Copolymerization of Ethylene and 4-Bromostyrene. The ^{13}C NMR spectra (Figure 10) of the ethylene + 4-bromostyrene copolymers share an almost identical pattern to the ethylene−styrene copolymers in the aliphatic region. In the aromatic region, the chemical shifts of the *ipso* and *para* carbons shift to δ = 145.3 and 119.7 ppm, respectively. As for the comonomer incorporation level, ^{1}H NMR spectra reveal that $\mathbf{Ti_2} + \mathbf{B_1}$ enchains 16.9 mol % 4-bromostyrene, which is 31.0% more than does $\mathbf{Ti_1} + \mathbf{B_1}$ (12.9 mol %). As a result, the T_g of the copolymers increases from 36.0 to 48.4 °C.

III. Copolymerization of Ethylene and Styrene by Mononuclear and Binuclear Organozirconium Catalysts. Copolymerization of ethylene and styrene in the presence of organozirconium catalysts was also investigated. Although CGCZr catalysts ($\mathbf{Zr_1}$, $\mathbf{Zr_2}$, and $\mathbf{C1\text{-}Zr_2}$) are competent for both ethylene[5b,h] and styrene homopolymerizations (see more below), attempts to effect ethylene−styrene copolymerization were unsuccessful, yielding only heterogeneous polyethylene and polystyrene mixtures (Figure 11). In addition, with increasing styrene:ethylene feed ratios, the percentage of polystyrene in the obtained polymeric product increases accordingly. Copolymerization of ethylene and styrene at both elevated and decreased polymerization temperatures, trying to depress the homopropagation selectivity, also failed, again producing mixtures of homopolymers. This is in agreement with previous

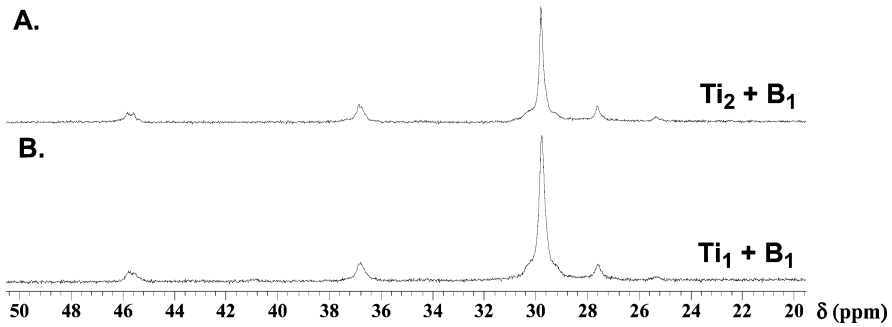

Figure 10. ^{13}C NMR spectra (100 MHz, $C_2D_2Cl_4$, 130 °C) of the poly(ethylene-*co*-4-bromostyrene) samples from Table 1, entries 10−11, in which the catalyst nuclearity is varied.

Table 2. Styrene Homopolymerization Results[a]

entry	cat. + cocat.	time (h)	yield (g)	activity[b] (×10^5)	T_g[c] (°C)	T_m[c] (°C)	M_w[e] (×10^4)	M_w/M_n[e]
1	**Ti_1 + B_1**	3	0.08	0.03	104.6	n.o.[d]	1.96	1.9
2	**Ti_2 + B_1**	3	3.13	1.04	96.4	n.o.[d]	1.04	1.6
3	**C1−Ti_2 + B_1**	2	3.93	1.96	94.6	n.o.[d]	0.64	2.6
4	**Ti_1 + B_2**	3	0.06	0.02	100.5	n.o.[d]	1.21	1.7
5	**Ti_2 + B_2**	3	3.36	1.12	89.2	n.o.[d]	0.80	1.5
6	**Zr_1 + B_1**	2	1.09	0.54	101.2	n.o.[d]	1.30	1.6
7	**Zr_2 + B_1**	2	3.91	1.96	94.2	n.o.[d]	1.02	1.6
8	**C1−Zr_2 + B_1**	1	4.07	4.07	93.1	n.o.[d]	0.70	2.7

[a] [M] = 10 μmol + [B] = 10 μmol, 5 mL styrene + 25 mL toluene at 20 °C. [b] Units: g polymer/(mol metal·h). [c] DSC. [d] Not observed. [e] GPC relative to polystyrene standards.

observations that CGCZr catalysts are not efficient for ethylene + methylenecycloalkane copolymerization.[5b]

IV. Homopolymerization of Styrene and End Group Analysis. Previously, we communicated that under identical styrene homopolymerization conditions, bimetallic catalyst **Ti_2** exhibits ∼50 times greater activity than the analogous monometallic catalyst **Ti_1,** and end group analysis suggests that unusual 1,2-regiochemistry is installed in ∼50% of the initiation steps. Here, we extended our studies to the methylene-bridged bimetallic catalyst **C1-Ti_2** and the organozirconium analogues **C1-Zr_2**, **Zr_2**, and **Zr_1** to study the effects of metal−metal proximity on the cooperative bimetallic effect. As illustrated in Table 2, under identical styrene polymerization conditions, **C1-Ti_2** + **B_1** and **Ti_2** + **B_1** exhibit ∼65 and ∼50 times greater homopolymerization activities than does monometallic **Ti_1** + **B_1**, respectively. Furthermore, **C1-Zr_2** + **B_1** and **Zr_2** + **B_1** exhibit ∼8 and ∼4 times greater activities, respectively, than does monometallic **Zr_1** + **B_1**. The monomodal GPC traces together with polydispersities ∼2 and end group analyses (see more below) suggest that all of the polystyrene homopolymers are produced exclusively via a coordinative/insertive single-site pathway. The marginal activity of mononuclear catalyst **Ti_1** is thought to arise from the "back-coordination" of the last inserted styrene (**A**), which prevents incoming monomer coordination and enchainment, while mononuclear **Zr_1** exhibits respectable styrene polymerization activity. This disparity in styrene homopolymerization activity argues that the more open coordination sphere of Zr here is better able to overcome the "back-coordination". The aforementioned trends in styrene homopolymerization activities for both organotitanium and organozirconium catalysts (**C1-M_2** > **M_2** > **M_1**) most likely reflect enhanced intramolecular cooperative effects with increased metal−metal proximity as the second metal center is poised to disrupt styrene "back-coordination" to the first metal center (Scheme 4). Interestingly, the molecular weights and glass transition temperatures of the product polystyrenes exhibit the opposite trend from activities: **C1-M_2** < **M_2** < **M_1**, suggesting functionally different propagation/termination kinetics (Table 2). Furthermore, organozirconium catalysts always exhibit greater activities than the corresponding organotitanium catalysts of the same nuclearity and afford comparable molecular weight polystyrene, in sharp contrast to ethylene homopolymerizations, where organotitanium catalysts exhibit far greater activities and afford much higher molecular weight polyethylenes than the corresponding organozirconium catalysts.

Scheme 4. Proposed Mechanism for Bimetallic Styrene Insertion Regiochemistry

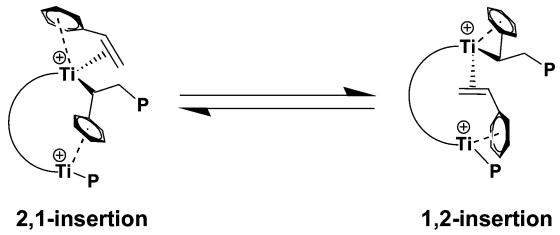

Regarding styrene insertion regiochemistry,[20] Scheme 5 depicts all possible end groups produced during the initiation steps in styrene homopolymerization. As can be seen from Figure 12,[26] **C1-Ti_2** and **Ti_2** share very similar end group

(24) For theoretical studies on styrene homopolymerization, see: (a) Yang, S. H.; Huh, J.; Jo, W. H. *Organometallics* **2006**, *25*, 1144−1150. (b) Yang, S. H.; Huh, J.; Yang, J. S.; Jo, W. H. *Macromolecules* **2004**, *37*, 5741−5751. (c) Nifant'ev, I. E.; Ustynyuk, L. Y.; Besedin, D. V. *Organometallics* **2003**, *22*, 2619−2629. (d) Minieri, G.; Corradini, P.; Guerra, G.; Zambelli, A.; Cavallo, L. *Macromolecules* **2001**, *34*, 5379−5385. (e) Minieri, G.; Corradini, P.; Zambelli, A.; Guerra, G.; Cavallo, L. *Macromolecules* **2001**, *34*, 2459−2468.

(25) For studies of styrene coordination with cationic metal center, see: (a) Kaminsky, W.; Lenk, S.; Scholtz, V.; Roesky, H. W.; Herzog, A. *Macromolecules* **1997**, *30*, 7647−7650. (b) Flores, J. C.; Wood, J. S.; Chien, J. C. W.; Rausch, M. D. *Organometallics* **1996**, *15*, 4944−4950. (c) Grassi, A.; Zambelli, A.; Laschi, F. *Organometallics* **1996**, *15*, 480−482.

(26) For polystyrene end group analysis, see: (a) Caporaso, L.; Izzo, L.; Sisti, I.; Oliva, L. *Macromolecules* **2002**, *35*, 4866−4870. (b) Zambelli, A.; Longo, P.; Pellecchia, C.; Grassi, A. *Macromolecules*, **1987**, *20*, 2035−2037. (c) Sato, H.; Tanaka, Y. *Macromolecules* **1984**, *17*, 1964−1966.

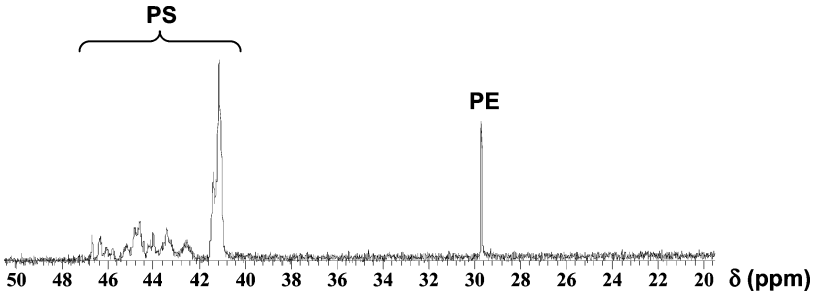

Figure 11. Representative ^{13}C NMR spectrum (100 MHz, $C_2D_2Cl_4$, 130 °C) of the polymeric product in ethylene−styrene copolymerization mediated by CGCZr catalysts.

Scheme 5. Possible Styrene Insertion Pathways during Chain Initiation

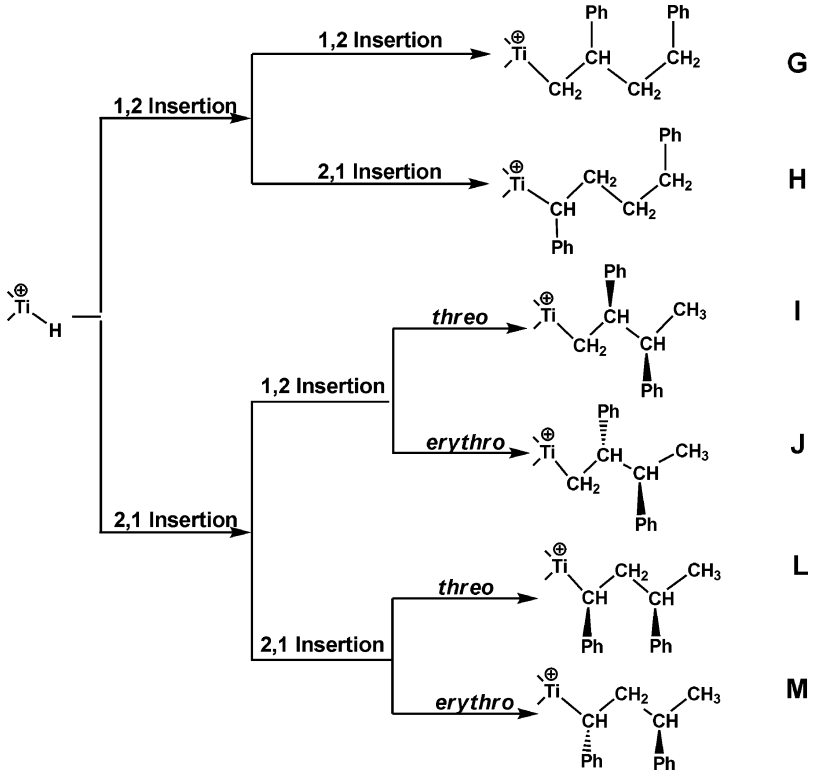

distributions, installing 1,2-insertion regiochemistry in ∼50% of all initiations. Interestingly, when the CGCZr-based catalysts are changed from $\mathbf{Zr_1}$ to $\mathbf{Zr_2}$ and $\mathbf{C1\text{-}Zr_2}$, an increasing percentage of 2,1-insertion regiochemistry is installed (Figure 13). This is in agreement with the proposed mechanism, that is, although mononuclear catalysts have strongly preferred styrene insertion regiochemistries (2,1-insertion for organotitanium,[20a,d,e] 1,2-insertion for organozirconium[26a]), the bimetallic catalytic environments tend to moderate the opposite Ti vs Zr selectivities in insertion regiochemistry.

V. Polar Solvent Effects. Previously reported $\mathbf{Ti_1}$- and $\mathbf{Ti_2}$-mediated ethylene + α-olefin copolymerization results[5a,b] in a more polar, ion pair weakening medium suggested that the proposed agostic interactions can be suppressed by polar C_6H_5Cl ($\epsilon_r = 5.68$ vs $\epsilon_r = 2.38$ for toluene),[29] as evidenced by the diminished comonomer enchainment efficiency of $\mathbf{Ti_2}$. However, such polar solvent effects might not be suppressed in the present styrene polymerizations since the metal-arene interactions in the proposed mechanistic scenario may be stronger than the C−H agostic interactions in α-olefin polymerizations. As shown in Table 3, the data on ethylene−styrene copolymerizations mediated by both $\mathbf{Ti_2}$ and $\mathbf{Ti_1}$ in C_6H_5Cl reveal that substantial amounts of atactic polystyrene are coproduced in addition to

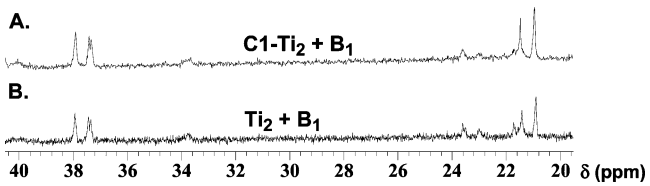

Figure 12. ^{13}C NMR end group analysis (100 MHz, $C_2D_2Cl_4$, 130 °C) of the polystyrenes from Table 2, entries 2−3.

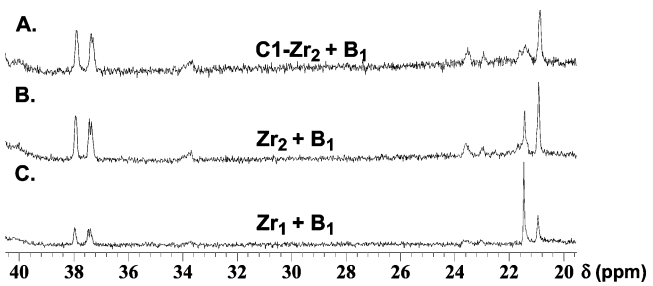

Figure 13. ^{13}C NMR end group analysis (100 MHz, $C_2D_2Cl_4$, 130 °C) of the polystyrenes from Table 2, entries 6−8.

Table 3. Copolymerization of Ethylene and Styrene in C_6H_5Cl with Cocatalyst $\mathbf{B_1}$[a]

entry	cat.	time (min)	yield (g)	PS wt %[b]	activity[c] (×10^6)	T_g[d] (°C)	T_m[d] (°C)	M_w[f] (×10^5)	M_w/M_n[f]	styrene%[g] (mol %)
1	$\mathbf{Ti_2}$	40	4.85	79.7	1.4	9.2	n.o.[e]	3.49	2.4	28.5
2	$\mathbf{Ti_1}$	18	3.06	55.4	2.0	−3.9	n.o.	4.62	1.8	21.7

[a] [Ti] = 5 μmol + [B] = 5 μmol, 10 mL styrene + 50 mL chlorobenzene at 20 °C. [b] Determined from solvent fractionation. [c] Units: g polymer/(mol Ti·atm ethylene·h). [d] By DSC. [e] Not observed. [f] By GPC relative to polystyrene standards. [g] Calculated from ^{1}H NMR.

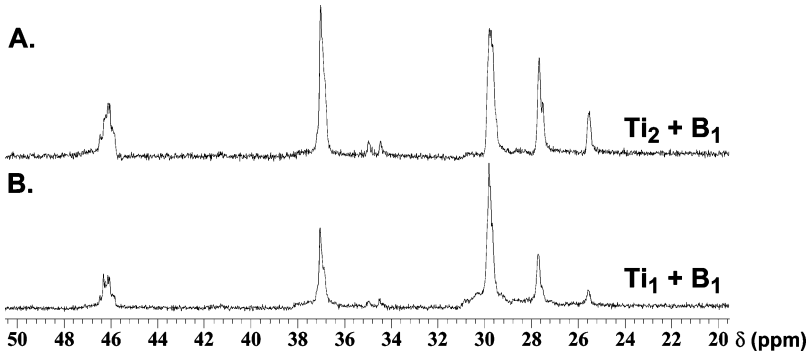

Figure 14. ^{13}C NMR spectra (100 MHz, $C_2D_2Cl_4$, 130 °C) of two poly(ethylene-*co*-styrene) samples from Table 4.

poly(ethylene-*co*-styrene), in sharp contrast to copolymerization results carried out in toluene where only copolymers are obtained. After removing the atactic polystyrene via solvent fractionation with methyl ethyl ketone (MEK), ^{13}C NMR data (Figure 14) reveal that the styrene incorporation levels for both $\mathbf{Ti_2}$ and $\mathbf{Ti_1}$ are significantly depressed in comparison to the copolymerization results in toluene, largely due to the decreased styrene:ethylene feed ratio arising from the coproduction of atactic polystyrene (depletion of styrene). Note that there are negligible solubility differences for ethylene in toluene and chlorobenzene under the present polymerization conditions.[30] Interestingly, although the effective styrene:ethylene feed ratio for $\mathbf{Ti_2}$ is lower than that for $\mathbf{Ti_1}$, because the former produces more atactic polystyrene, $\mathbf{Ti_2}$ still incorporates 31.3% more styrene than $\mathbf{Ti_1}$, while in toluene $\mathbf{Ti_2}$ only enchains 15.4% more styrene than $\mathbf{Ti_1}$. It can therefore be seen that this bimetallic selectivity effect is actually enhanced in the polar solvent, arguing that any C_6H_5Cl coordination cannot compete with the metal−arene interaction.

VI. Synthesis, Characterization, and Activation Studies of the Model Compound $\mathbf{Ti_2(CH_2Ph)_4}$. To further probe the proposed enchainment mechanism in **C1-Ti$_2$** and $\mathbf{Ti_2}$-mediated styrene homopolymerization involving one cationic metal center interacting with the phenyl ring of the last inserted styrene on the other cationic metal center, thus preventing "back-coordination" and deactivation of the electrophilic metal center, model compound $\mathbf{Ti_2(CH_2Ph)_4}$ was designed to simulate bimetallic Ti-polymeryl species after cocatalyst alkyl abstraction. Initial attempts to synthesize the title complex via direct protonolytic alkane elimination[31] were unsuccessful, presumably due to the sterically demanding environment of the bimetallic CGC ligand structure (Scheme 6). Thus, more conventional methodology was employed.[32,33] As illustrated in Scheme 6, reaction of known $\mathbf{Ti_2(NMe_2)_4}$[5a] with excess Me_3SiCl at room temperature cleanly affords the tetrachloro complex $\mathbf{Ti_2Cl_4}$. Subsequent reaction with $PhCH_2MgCl$ affords the tetrabenzyl complex $\mathbf{Ti_2(CH_2Ph)_4}$, which was characterized by standard spectroscopic and analytical techniques, as well as by X-ray diffraction (vide infra).

In the ^{1}H NMR spectrum of $\mathbf{Ti_2(CH_2Ph)_4}$, the methylene protons of the two magnetically nonequivalent diastereotopic benzyl proton pairs appear as two AB spin patterns with $^2J_{H-H}$ coupling constants ∼10.5 Hz. The *ortho* protons of the benzyl groups exhibit normal resonances at δ = 6.71 and 6.62 ppm, respectively.[19d,33a,c] The ^{13}C{^{1}H} NMR spectrum reveals two distinct signals at δ = 84.90 and 80.23 ppm, respectively, corresponding to the two nonequivalent methylene carbons of the magnetically nonequivalent benzyl groups. Furthermore, the *ipso* carbons of the benzyl groups are found to exhibit normal chemical shifts at δ = 150.09 and 146.58 ppm, respectively. Unlike those reported for some neutral multihapto metal-benzyl complexes,[33] the aforementioned NMR spectroscopic evidence as well as the solid-state structural data (see more below) suggest

(27) For theoretical studies on monomer insertion in ethylene−styrene copolymerizations, see: (a) Ramos, J.; Muñoz-Escalona, A.; Martínez, S.; Martínez-Salazar, J.; Cruz, V. *J. Chem. Phys.* **2005**, *122*, 074901/1−074901/4. (b) Yokota, K.; Kohsaka, T.; Ito, K.; Ishihara, N. *J. Polym. Sci., Part A: Polym. Chem.* **2005**, *43*, 5041−5048. (c) Martínez, S.; Exposito, M. T.; Ramos, J.; Cruz, V.; Martínez, M. C.; López, M.; Muñoz-Escalona, A.; Martínez-Salazar, J. *J. Polym. Sci., Part A: Polym. Chem.* **2005**, *43*, 711−725. (d) Martínez, S.; Cruz, V.; Muñoz-Escalona, A.; Martínez-Salazar, J. *Polymer* **2003**, *44*, 295−306. (e) Yang, S. H.; Jo, W. H.; Noh, S. K. *J. Chem. Phys.* **2003**, *119*, 1824−1837. (f) Muñoz-Escalona, A.; Cruz, V.; Mena, N.; Martínez, S.; Martínez-Salazar, J. *Polymer* **2002**, *43*, 7017−7026. (g) Oliva, L.; Caporaso, L.; Pellecchia, C.; Zambelli, A. *Macromolecules* **1995**, *28*, 4665−4667.
(28) (a) Hong, S.; Marks, T. J. *Acc. Chem. Res.* **2004**, *37*, 673−686. (b) Gagne, M. R.; Stern, C. L.; Marks, T. J. *J. Am. Chem. Soc.* **1992**, *114*, 275−294.
(29) (a) Bouwkamp, M. W.; de Wolf, J.; del Hierro Morales, I.; Gercama, J.; Meetsma, A.; Troyanov, S. I.; Hessen, B.; Teuben, J. H. *J. Am. Chem. Soc.* **2002**, *124*, 12956−12957. (b) Kawabe, M.; Murata, M. *Macromol. Chem. Phys.* **2001**, *202*, 2440−2446. (c) Rybtchinski, B.; Konstantinovsky, L.; Shimon, L. J. W.; Vigalok, A.; Milstein, D. *Chem.−Eur. J.* **2000**, *6*, 3287−3292. (d) Carr, N.; Mole, L.; Orpena, A. G.; Spencer, G. L. *J. Chem. Soc., Dalton Trans.* **1992**, *18*, 2653−2662. (e) Peng, T. S.; Gladysz, J. A. *J. Am. Chem. Soc.* **1992**, *114*, 4174−4181. (f) Agbossou, S. K.; Bodner, G. S.; Patton, A. T.; Gladysz, J. A. *Organometallics* **1990**, *9*, 1184−1191. (g) Schmidt, G. F.; Brookhart, M. *J. Am. Chem. Soc.* **1985**, *107*, 1443−1444.
(30) The solubility of ethylene is reported to be 0.117 mol/L in toluene[30a] and 0.118 mol/L in chlorobenzene[30b] under the present polymerization conditions (25 °C, 1.0 atm): (a) Atiqullah, M.; Hammawa, H.; Hamid, H. *Eur. Polym. J.* **1998**, *34*, 1511−1520. (b) Sahgal, A.; La, H. M.; Hayduk, W. *Can. J. Chem. Eng.* **1978**, *56*, 354−357.
(31) Chen, Y. X.; Marks, T. J. *Organometallics* **1997**, *16*, 3649−3657.
(32) (a) Amor, F.; Butt, A.; du Plooy, K. E.; Spaniol, T. P.; Okuda, J. *Organometallics* **1998**, *17*, 5836−5849. (b) Amor, F.; Okuda, J. *J. Organomet. Chem.* **1996**, *520*, 245−248.
(33) (a) Latesky, S. L.; McMullen, A. K.; Niccolai, G. P.; Rothwell, I. P.; Huffman, J. C. *Organometallics* **1985**, *4*, 902−908. (b) Lubben, T. V.; Wolczanski, P. T.; Van Duyne, G. D. *Oganometallics* **1984**, *3*, 977−983. (c) Mintz, E. A.; Moloy, K. G.; Marks, T. J.; Day, V. W. *J. Am. Chem. Soc.* **1982**, *104*, 4692−4695. (d) Wolczanski, P. T.; Bercaw, J. E. *Organometallics* **1982**, *1*, 793−799.

Scheme 6. Synthetic Route to Model Compound $\mathbf{Ti_2(CH_2Ph)_4}$

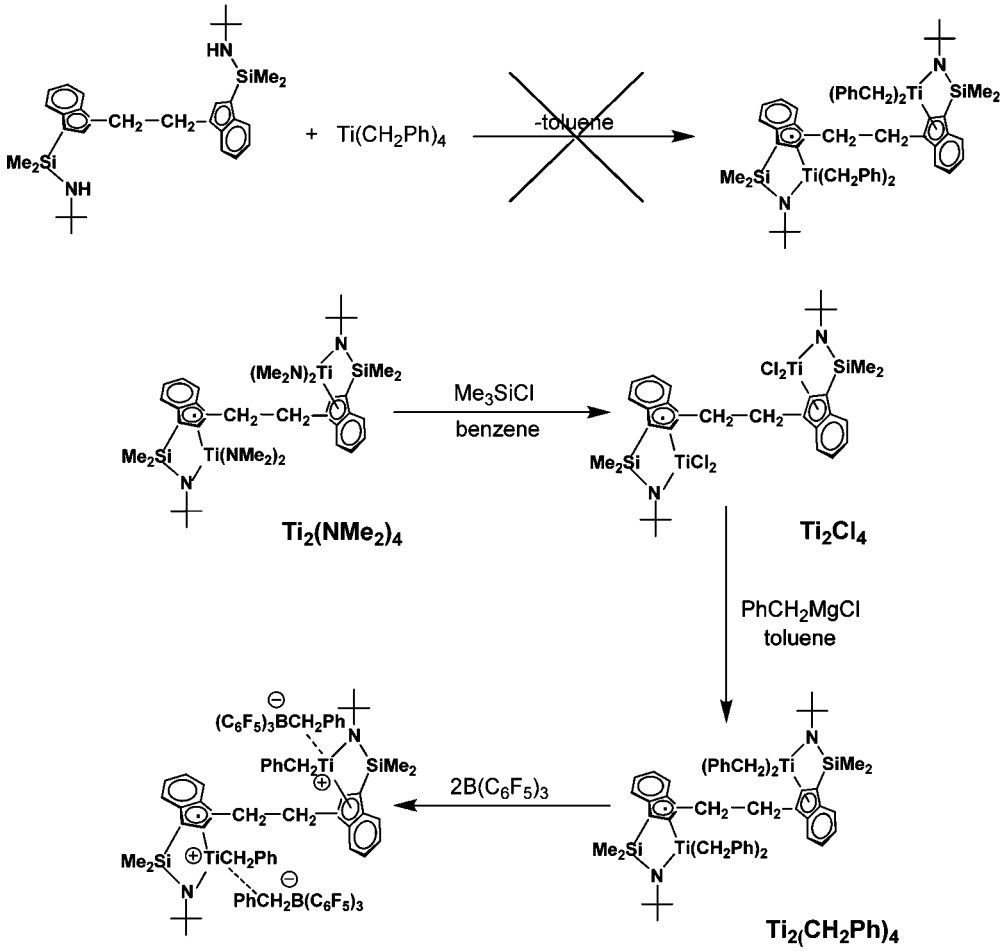

that for $\mathbf{Ti_2(CH_2Ph)_4}$, all of the benzyl groups engage in an η^1-coordination mode both in solution and in the solid state.

Although mixing $\mathbf{Ti_2(CH_2Ph)_4}$ and 2 equiv of $B(C_6F_5)_3$ in benzene-d_6 immediately results in the formation of dark-red solids, and ^{1}H NMR spectroscopy indicates clean double-benzyl abstraction by the cocatalyst/activator, attempts to isolate the pure crystalline bimetallic ion pair complex were unsuccessful, most likely due to rapid thermal decomposition within hours, as monitored by ^{1}H NMR spectroscopy. Interestingly, among the three possible diastereomeric double benzyl abstraction products, only one of the two C_i-symmetric ion pair complexes could be identified, because only a single set of upfield-shifted ligand resonances was observed. This preferential reactivity of $B(C_6F_5)_3$ with one of the two inequivalent benzyl groups is in sharp contrast to parallel activation studies of $\mathbf{Ti_1}$, where both possible ion pair complex isomers are observed in solution.[5a] The diastereotopic benzylic proton pairs of the two isomeric cationic Ti centers still exhibit AB spin patterns, evidenced by two sets of doublets centered at $\delta = 2.91$ and 2.43 ppm with an average $^2J_{H-H} \approx 8.0$ Hz. This decrease in the chemical shift difference between the two benzylic hydrogens ($\Delta\delta = 0.48$ after activation vs $\Delta\delta = 1.63$ before activation) provides evidence for an η^1-$PhCH_2Ti^+$ coordination mode, because η^n-$PhCH_2Ti^+$ bonding should plausibly make the two benzylic protons more magnetically inequivalent and therefore increase the chemical shift difference.[19d] The decrease in coupling constant (cf., $\mathbf{Ti_2(CH_2Ph)_4}$: $^2J_{H-H} = 10.5$ Hz) most likely reflects an α-agostic interaction between the electrophilic Ti center and a benzylic C−H bond, which is thought to stabilize cationic metal centers during olefin polymerization.[6c,34] More importantly, this $^2J_{H-H}$ reduction as well as normal Ti^+CH_2Ph *ortho* proton chemical shifts[19d,33a,c] also argue against the possibility of dominant η^n-$PhCH_2Ti^+$ coordination, which is expected to increase the sp^2 character of the benzylic carbon and thus increase $^2J_{H-H}$.[33] The fact that only one broad ^{1}H resonance at $\delta = 3.62$ ppm is observed for the BCH_2Ph protons and that no signal in the range of $\delta = 5-6$ ppm is observed for the BCH_2Ph *ortho* protons argues that η^1-$PhCH_2B(C_6F_5)_3^-$ bonding also predominates.[31]

VII. Molecular Structure of Model Compound $\mathbf{Ti_2(CH_2Ph)_4}$. A summary of crystal structure data for the complex $\mathbf{Ti_2(CH_2Ph)_4}$ is presented in Table 4, and selected bond distances and angles for $\mathbf{Ti_2(CH_2Ph)_4}$ are summarized in Table 5. Similar to the previously reported molecular structure of $\mathbf{Ti_2(NMe_2)_4}$, the crystal structure of $\mathbf{Ti_2(CH_2Ph)_4}$ (Figure 15) reveals an inversion center with a CGCTi moiety located on either side of the ethylenebis(indenyl) fragment and with the two π-coordinated indenyl rings in a diastereomeric relationship. As can be seen from Figure 15, the crystal consists of a single diastereomer (*SR*, *RS*). The bond angles C(15)−C(14)−Ti(1) = 126.12(18)° and C(8)−C(7)−Ti(1) = 117.79(18)° suggest that all of the benzyl groups exhibit an η^1-coordination mode, since η^n-$PhCH_2Ti$ coordination would bend the phenyl moiety close to the metal center and consequently afford substantially

(34) (a) Mashima, K.; Nakamura, A. *J. Organomet. Chem.* **1992**, *428*, 49−58. (b) Brookhart, M.; Green, M. L. H. *J. Organomet. Chem.* **1983**, *250*, 395−408.

Table 4. Summary of Crystal Structure Data for $\mathbf{Ti_2(CH_2Ph)_4}$[a]

empirical formula	$C_{62.50}H_{76}N_2Si_2Ti_2$
formula weight	1007.23
crystal color, habit	red, block
crystal dimensions (mm)	0.520 × 0.424 × 0.374
crystal system	triclinic
space group	$P\bar{1}$
a, Å	12.299(2)
b, Å	16.117(3)
c, Å	16.873(3)
α, deg	97.363(3)
β, deg	101.480(3)
γ, deg	112.119(2)
V, Å^3	2959.5(8)
Z	2
d (calcd), g/cm^3	1.130
μ, mm^{-1}	0.348
$T_{min} - T_{max}$	0.8481−0.8912
measured reflections	15176
independent reflections	15176
reflections > 2*σ* (*I*)	12744
R_{int}	0.0000
$R[F^2 > 2\sigma(F^2)]$	0.0655
$wR(F^2)$	0.1894
S	1.038
no. of parameters	653

[a] Conditions: CCD area detector diffractometer; *ψ* and *ω* scans; temperature for data collection 153(2) K; Mo Kα radiation; *λ* = 0.71073 Å.

Table 5. Selected Bond Distances (Å) and Bond Angles (deg) for $\mathbf{Ti_2(CH_2Ph)_4}$

Bond Distances			
Ti(1)−C(21)	2.498(3)	C(14)−C(15)	1.493(4)
Ti(1)−C(22)	2.341(2)	Ti(1)−N(1)	1.931(2)
Ti(1)−C(23)	2.271(2)	Si(1)−N(1)	1.753(2)
Ti(1)−C(24)	2.413(2)	Si(1)−C(1)	1.870(3)
Ti(1)−C(29)	2.564(3)	Si(1)−C(2)	1.853(3)
Ti(1)−C(7)	2.154(3)	Si(1)−C(23)	1.854(3)
Ti(1)−C(14)	2.132(3)	N(1)−C(3)	1.486(3)
C(7)−C(8)	1.480(4)		
Bond Angles			
N(1)−Ti(1)−C(14)	106.42(10)	N(1)−Si(1)−C(23)	93.54(10)
N(1)−Ti(1)−C(7)	117.39(10)	C(2)−Si(1)−C(1)	108.26(15)
C(14)−Ti(1)−C(7)	99.55(11)	C(1)−Si(1)−C(23)	112.45(13)
C(15)−C(14)−Ti(1)	126.12(18)	C(2)−Si(1)−C(23)	110.22(13)
C(8)−C(7)−Ti(1)	117.79(18)	C(3)−N(1)−Si(1)	124.59(17)
N(1)−Si(1)−C(1)	116.89(13)	C(3)−N(1)−Ti(1)	133.74(17)
N(1)−Si(1)−C(2)	114.77(12)	Si(1)−N(1)−Ti(1)	101.58(10)
C(15)−C(14)−Ti(1)	126.12(18)	C(8)−C(7)−Ti(1)	117.79(18)

smaller bond angles (<90°).[19a,b,c,f,i,j,k] The sum of the bond angles around nitrogen atom N(1) is 359.91°, indicating that the formal hybridization of nitrogen atom N(1) is sp^2. The ^{t}-BuN−Ti bond distance (Ti(1)−N(1)) is 1.931(2) Å, substantially shorter than the one reported for $\mathbf{Ti_2(NMe_2)_4}$ (1.994(4) Å), largely due to increased *π* donation from the N formal lone pair electrons to the empty Ti^{4+} *d* orbitals since no additional nitrogen atoms are engaged in *π* donation. The sum of bond angles around indenyl ring carbon atom C(23) is 351.2°, indicating that the C(23)−Si(1) bond deviates appreciably from the indenyl ring plane because of the constrained geometry. The carbon atoms of the Cp ring do not exhibit equal bonding distances to the Ti center. The average bond lengths of Ti(1)−C(22)/Ti(1)−C(23) and Ti(1)−C(21)/Ti(1)−C(24)/Ti(1)−C(29) are 2.306(2) and 2.492(3) Å, respectively. The difference is 0.186(5) Å, 0.018(14) Å greater than the value reported for the Cp ligand in $\mathbf{Ti_2(NMe_2)_4}$ [2.542(5) − 2.374(4) = 0.168(9) Å],[5a] and 0.055 Å greater than that value found for the more symmetrical Cp ligand in $[(\eta^5\text{-}C_5Me_4)SiMe_2(^tBuN)]TiCl_2$, which is 2.436 − 2.305 = 0.131 Å,[35] indicating a substantially more "slipped" coordination of the Cp ligand in $\mathbf{Ti_2(CH_2Ph)_4}$.

Discussion

I. Bimetallic Proximity Effects in Polymerization. From the polymerization results outlined above, the enhanced styrene incorporation in **C1-Ti$_2$**- vs **Ti$_2$**-mediated ethylene−styrene copolymerizations, and the significantly enhanced activities in **C1-M$_2$**- vs **M$_2$**-mediated styrene homopolymerizations (M = Ti and Zr), suggest that **C1-M$_2$** structures exhibit enhanced metal−metal cooperativity effects compared to **M$_2$**. It is known that in the single-crystal structure of C_1-symmetric **C1-Zr$_2$**,[5b] the two indenyl rings are locked (estimated rotation barrier >63 kcal/mol, Spartan 2002, MP3 level) into a twisted conformation by the methylene bridge, constraining the two metal centers to the same side of the molecule,[5b] whereas in the solid-state structure of C_i-symmetric **Zr$_2$**, the two Zr atoms reside on opposite sides of the molecule but with minimal estimated barriers to accessing other conformations. As a result, the minimum accessible Zr···Zr distance in **C1-Zr$_2$** (7.392 Å) is ∼1.28 Å shorter than that in **Zr$_2$** (8.671 Å).[5b] Therefore, the locked and shorter accessible metal−metal distance in the case of **C1-M$_2$** would enable more efficient binuclear metal-styrene binding (Scheme 4), hence affording more efficient comonomer enchainment and greater styrene homopolymerization activity than **M$_2$**. A similar trend has been reported for ethylene + 1-hexene copolymerizations, where **C1-Zr$_2$** incorporates more 1-hexene than does **Zr$_2$** under identical reaction conditions.[5b]

II. Comparison of CGCTi and CGCZr Catalytic Properties. In the aforementioned styrene homopolymerization studies, CGCZr-based catalysts exhibit far greater activities than do CGCTi-based catalysts having the same nuclearity and afford polymeric products with comparable molecular weights. In contrast, for polymerizations involving ethylene, organotitanium catalysts generally exhibit far greater activities and afford much higher molecular weight polyethylenes than do analogous organozirconium catalysts. It is known that for ethylene polymerizations, coordination of ethylene to the cationic metal center in the presence of the counteranion is usually the rate-determining step for each ethylene insertion,[36] while for styrene polymerizations, insertion of the coordinated styrene into the metal-polymeryl bond is thought to be the rate-determining step.[24b] Theoretical studies regarding ethylene−styrene copolymerizations[27a,c,e] as well as experimental results[23b] also reveal that ethylene has a lower complexation energy than does styrene while the latter has a significantly higher insertion barrier than the former. DFT calculations also suggest that solvent molecules are much more likely to compete with ethylene for coordination to CGCZr than to CGCTi,[37] and therefore, CGCTi is expected to have more efficient ethylene coordination and subsequent insertion. Moreover, tighter ion pairing in CGCZr versus CGCTi[38] also makes ethylene coordination to CGCZr,

(35) Carpenetti, D. W.; Kloppenburg, L.; Kupec, J. T.; Petersen, J. L. *Organometallics* **1996**, *15*, 1572−1581.
(36) (a) Motta, A.; Fragalà, I. L.; Marks, T. J. *J. Am. Chem. Soc.* **2007**, *129*, 7327−7338. (b) Xu, Z.; Vanka, K.; Ziegler, T. *Organometallics* **2004**, *23*, 104−116. (c) Nifant'ev, I. E.; Ustynyuk, L. Y.; laikov, D. N. *Organometallics* **2001**, *20*, 5375−5393.
(37) Chan, M. S. W.; Vanka, K.; Pye, C. C.; Ziegler, T. *Organometallics* **1999**, *18*, 4624−4636.
(38) Luo, L.; Marks, T. J. *Top. Catal.* **1999**, *7*, 97−106.

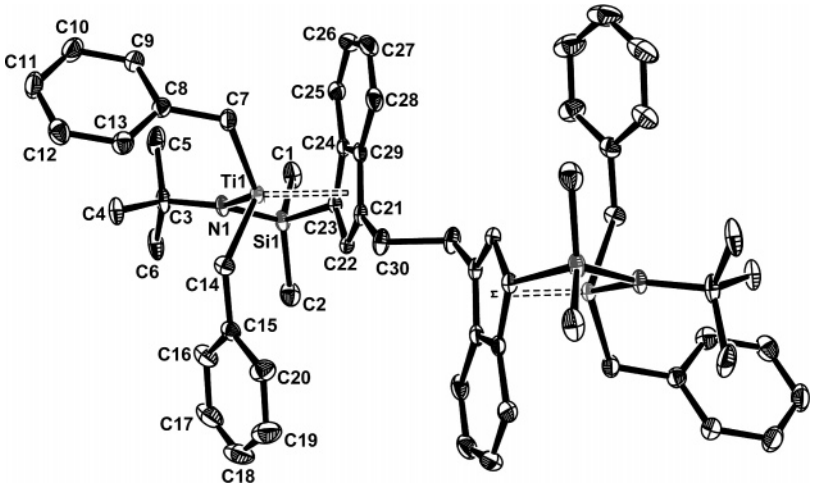

Figure 15. The molecular structure and atom numbering scheme for the model compound $\mathbf{Ti_2(CH_2Ph)_4}$. Thermal ellipsoids are drawn at the 30% probability level.

Scheme 7. Pathways for Styrenic Comonomer Enchainment in Bimetallic Catalyst-Mediated Ethylene Copolymerization

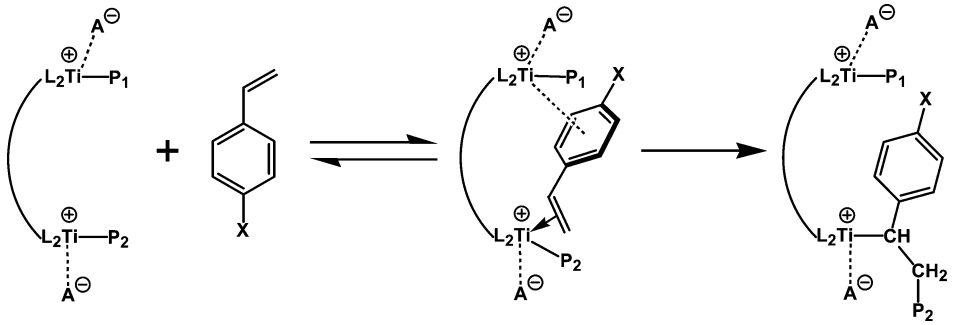

by displacing the counteranion, more energetically demanding. On the other hand, insertion of styrene into the metal−polymeryl bond is a sterically more sensitive process, and thus CGCZr with a larger ionic radius should promote more rapid enchainment, all other factors being equal. This trend is similar to that observed for organolanthanide-catalyzed intramolecular aminoalkene hydroamination/cyclization, where the cyclization rate increases with increasing lanthanide radius since olefin insertion is turnover-limiting.[28]

Unlike their CGCTi counterparts which are competent for efficient ethylene−styrene copolymerization, under the reaction conditions investigated, all of the three CGCZr catalysts ($\mathbf{C_1}$-Zr_2, $\mathbf{C_2}$-Zr_2, and $\mathbf{Zr_1}$) fail to produce ethylene−styrene copolymers although both monomers undergo homopolymerization at these Zr centers. As a matter of fact, very few Zr-based catalysts[9j,21b] are reported in the literature to efficiently copolymerize ethylene and styrene. This difference in the catalytic comonomer incorporation selectivity was previously observed in our work on isobutene, methylenecyclopentane, and methylenecyclohexane copolymerizations with ethylene: CGCTi catalysts incorporate significant quantities of sterically encumbered comonomers into polyethylene backbones, whereas CGCZr catalysts do not. One plausible explanation is that tighter ion pairing in CGCZr versus CGCTi structures leads to lower reactivity in terms of comonomer enchainment.[38]

III. Bimetallic Effects on Comonomer Enchainment. For all five styrenic comonomers investigated having various *para* substituents, under identical copolymerization conditions, binuclear catalyst $\mathbf{Ti_2} + \mathbf{B_1}$ invariably incorporates far greater levels of comonomer than does the mononuclear $\mathbf{Ti_1} + \mathbf{B_1}$ analogue, demonstrating the generality of the bimetallic effect previously observed only with styrene.[5e] It is proposed that coordination of the styrenic comonomer to a cationic metal center is stabilized by interactions between the π-system of the substituted/unsubstituted phenyl ring with the proximate cationic metal center, which may facilitate/stabilize comonomer capture/binding and enhance the subsequent enchainment probability (Schemes 4 and 7). The bimetallic effect, which is defined here as the relative comonomer enchainment selectivity difference between $\mathbf{Ti_2}$ and $\mathbf{Ti_1}$ (eq 10), is found to depend strongly on the arene substituent and, all other factors being equal

$$\text{Bimetallic Effect} = \frac{\%\ \text{Styrenic}(\mathbf{Ti_2}) - \%\text{Styrenic}(\mathbf{Ti_1})}{\%\text{Styrenic}(\mathbf{Ti_1})} \times 100\% \quad (10)$$

in the proposed model, would be expected to increase as the interaction between the arene π-system and the electrophilic metal center increased. Because all of the styrenic comonomers possess almost identical steric characteristics, it is reasonable to assume that the π-electron density on the phenyl ring would dominate the metal−arene interaction.

It is known that such metal−benzyl arene interactions primarily involve the benzylic *ipso* carbon,[19,33] and therefore, the bimetallic effect should track the *ipso* carbon π-electron density of the styrenic comonomer. As shown in Table 6, the observed bimetallic effect parallels the same trend as the electron density on the styrenic comonomer *ipso* carbon atom as qualitatively assayed by the ^{13}C NMR chemical shifts.[39] Although reactivity ratio data are not available for direct

Table 6. Correlation between the Bimetallic Effect ($\mathbf{Ti_2}$ vs $\mathbf{Ti_1}$ Comonomer Enchainment Selectivity) and *ipso* Carbon Chemical Shift of the Styrenic Comonomers

substituent	F	Cl	Br	Me	H
bimetallic effect	45.4%	41.2%	31.0%	28.9%	15.4%
δ_{ipso} (ppm)	136.34	136.62	136.99	137.93	138.29

comparison due to the lack of ethylene solubility data in some comonomers, the general observed trend is informative, and the results are consistent with the mechanistic picture proposed: the stronger the metal−arene interaction, the more efficiently $\mathbf{Ti_2}$ enchains the styrenic comonomer vs $\mathbf{Ti_1}$.

IV. Solvent Polarity Effects on Polymerization. It was reported previously[5a,b] that for ethylene + α-olefin copolymerizations carried out in polar C_6H_5Cl as the solvent, the comonomer enchainment level difference between bimetallic $\mathbf{M_2}$ catalysts and monometallic $\mathbf{M_1}$ catalysts (M = Ti for ethylene + methylenecyclopentane copolymerization;[5a] M = Zr for ethylene + 1-hexene copolymerization[5b]) diminishes since the polar solvent can compete for/coordinate to the electrophilic metal centers and weaken/replace agostic interactions,[29] which were proposed to be mechanistically central to the observed binuclear enchainment effects. The present copolymerization results in the same polar solvent argue that, operationally, the metal-arene interaction remains largely intact in C_6H_5Cl since the significant disparity of styrene incorporation levels between $\mathbf{Ti_2}$ and $\mathbf{Ti_1}$ remain almost unchanged. Indeed, it has been reported that the η^2-bonding mode of d^0 metal−benzyl species remains largely undisrupted in polar solvents such as 1,1,2,2-tetrachloroethane[19h] ($\epsilon_r = 8.2$) and methylene chloride[19i] ($\epsilon_r = 9.1$).

V. Activation Studies of Model Compound $\mathbf{Ti_2(CH_2Ph)_4}$. The design of the model compound $\mathbf{Ti_2(CH_2Ph)_4}$ is to simulate the growing polystyrene chain with the last styrene installed in a 2,1 fashion. Upon alkyl abstraction by the cocatalyst/activator $B(C_6F_5)_3$, the resulting bimetallic ion pair $\mathbf{[Ti_2(CH_2Ph)_2]^{2+}[PhCH_2B(C_6F_5)_3^-]_2}$ should closely resemble the bimetallic Ti-polymeryl propagating species. Although some neutral metal−benzyl complexes are reported to exhibit an η^n-coordination mode ($n > 1$) of the benzyl groups,[33] the benzyl groups of the model compound $\mathbf{Ti_2(CH_2Ph)_4}$, however, engage in an η^1-coordination mode both in solution and in the solid state, largely due to lack of coordinative unsaturation around the metal center. The significant styrene homopolymerization activity disparity between $\mathbf{Ti_2}$ and $\mathbf{Ti_1}$ most likely arises from, as proposed above, the preferential coordination of the phenyl ring of the last inserted styrene to the second metal center. Although definitive solution structural data (chemical shifts of the benzylic *ipso* carbons and $^1J_{C-H}$) as well as solid-state structure for the bimetallic ion pair are not available to confirm the interaction of the benzylic arene to the second metal center, the present polymerization results as well as spectroscopic evidence argue at least that, in the presence of a second electrophilic metal center, minimal monometallic "back-coordination" of the last inserted styrene to the parent cationic metal center occurs.

(39) (a) Casabianca, L. B.; De Dios, A. C. *J. Phys. Chem. A* **2006**, *110*, 7787−7792. (b) Termaten, A.; van der Sluis, M.; Bickelhaupt, F. *Euro J. Org. Chem.* **2003**, *11*, 2049−2055. (c) Stothers, J. B. In *Carbon-13 NMR Spectroscopy*; Academic Press: New York, 1972; pp 90−91. (d) Nelson, G. L.; Levy, G. C.; Cargioli, J. D. *J. Am. Chem. Soc.* **1972**, *94*, 3089−3094. (e) Spiesecke, H.; Schneider, W. G. *J. Chem. Phys.* **1961**, *35*, 731−738.

Conclusions

The results of the present study significantly expand the scope of applicable comonomers in binuclear CGC olefin polymerization catalysis. In styrene homopolymerizations, bimetallic organotitanium catalysts (μ-CH_2-3,3′){(η^5-indenyl)[1-Me_2Si-(^{t}BuN)]($TiMe_2$)}$_2$ [MBICGC($TiMe_2$)$_2$; $\mathbf{C1\text{-}Ti_2}$] + $Ph_3C^+B(C_6F_5)_4^-$ ($\mathbf{B_1}$) and (μ-CH_2CH_2-3,3′){(η^5-indenyl)[1-Me_2Si(^{t}BuN)]($TiMe_2$)}$_2$ [EBICGC($TiMe_2$)$_2$; $\mathbf{Ti_2}$] + $\mathbf{B_1}$ exhibit ∼65 and ∼35 times greater activities, respectively, than does monometallic [1-Me_2-Si(3-ethylindenyl)(^{t}BuN)]$TiMe_2$ ($\mathbf{Ti_1}$) + $\mathbf{B_1}$. Bimetallic organozirconium catalysts (μ-CH_2-3,3′){(η^5-indenyl)[1-Me_2Si(^{t}BuN)]-($ZrMe_2$)}$_2$ [MBICGC($ZrMe_2$)$_2$; $\mathbf{C1\text{-}Zr_2}$] + $\mathbf{B_1}$ and (μ-CH_2CH_2-3,3′){(η^5-indenyl)[1-Me_2Si(^{t}BuN)]($ZrMe_2$)}$_2$ [EBICGC($ZrMe_2$)$_2$; $\mathbf{Zr_2}$] + $\mathbf{B_1}$ exhibit ∼8 and ∼4 times higher activities, respectively, than does monometallic [1-Me_2Si(3-ethylindenyl)(^{t}BuN)]-$ZrMe_2$ ($\mathbf{Zr_1}$) + $\mathbf{B_1}$. The binuclear catalysts exhibit significantly greater activities than the corresponding mononuclear catalysts, and more interestingly, as the minimum accessible distance between the adjacent metal centers decreases, this observed cooperative nuclearity effect increases in the following order: $\mathbf{C1\text{-}M_2} > \mathbf{M_2} > \mathbf{M_1}$ (M = Ti and Zr). In situ activation studies of the model compound $\mathbf{Ti_2(CH_2Ph)_4}$ suggest that under polymerization conditions, minimal monometallic "back-coordination" of the last inserted styrene to the parent cationic metal center occurs.

Increases in styrenic comonomer enchainment selectivity into the polyethylene microstructure for variously *para*-substituted styrenes are observed with binuclear catalyst $\mathbf{Ti_2} + \mathbf{B_1}$ versus the corresponding mononuclear catalyst $\mathbf{Ti_1} + \mathbf{B_1}$ under identical polymerization conditions. The relative magnitude of this bimetallic effect approximately mirrors the π-electron density at the *ipso* carbon: 4-fluorostyrene >4-chlorostyrene > 4-bromostyrene > 4-methylstyrene > styrene. Polar solvation is found to play a significant role in binuclear ion pairing, affording different polymeric products while not diminishing the bimetallic effect.

The results of this study indicate that multinuclear single-site polymerization catalysts can effect unusual cooperative enchainment processes involving comonomers which possess additional coordinating moieties and hence offer the potential of creating new macromolecular architectures which conventional monometallic catalysts cannot offer.

Acknowledgment. Financial support from NSF (Grant No. CHE-0415407) and DOE (Grant No. 86ER13511) is gratefully acknowledged. We thank Dr. E. Szuromi and Prof. R. F. Jordan of University of Chicago for generous help with the GPC measurements. N.G. thanks Dr. L. Li, Dr. H. Li, and Prof. J. B. Lambert for helpful discussions.

Supporting Information Available: Crystallographic data for $\mathbf{Ti_2(CH_2Ph)_4}$. This material is available free of charge via the Internet at http://pubs.acs.org.

JA076407M